이학박사학위논문

성호르몬에 의한 성체 근육 줄기세포의 형성에 관한 연구

Studies on the establishment of adult muscle stem cells by Sex hormones

2017년 2월

서울대학교 대학원

생명과학부

김 지 훈

성호르몬에 의한 성체 근육 줄기세포의 형성에 관한 연구

Studies on the establishment of adult muscle stem cells by Sex hormones

지도교수 공 영 윤

이 논문을 이학박사 학위논문으로 제출함
2017년 2월

서울대학교 대학원
생명과학부
김 지 훈

김지훈의 이학박사 학위논문을 인준함
2016년 12월

위 원 장 _____ (인)

부위원장 _____ (인)

위 원 _____ (인)

위 원 _____ (인)

위 원 _____ (인)

Studies on the establishment of adult muscle stem cells by Sex hormones

A dissertation submitted in partial
Fulfillment of the requirement for the degree of

DOCTOR OF PHILOSOPHY

To the Faculty of
School of Biological Sciences
at
SEOUL NATIONAL UNIVERSITY
By
Ji-Hoon Kim

Date Approved:

_____ _____

_____

_____

_____

_____

ABSTRACT

Studies on the establishment of adult muscle stem cells by Sex hormones at puberty

Ji-Hoon Kim
School of Biological Sciences
The Graduate School
Seoul National University

Quiescent satellite cells, known as adult muscle stem cells, possess a remarkable ability to regenerate skeletal muscle following injury throughout life. Active proliferation and differentiation of juvenile satellite cells contribute to myonuclear accretion in the pre-existing myofiber until puberty. Meanwhile, some of juvenile satellite cells preserve their stemness in order to comprise a reservoir of adult stem cells. Although it is known that they mainly originate from multipotent stem/progenitor cells of the somite, the mechanism underlying the establishment of quiescent satellite cell populations is unknown.

Stem cells interact with their specialized microenvironment which refers to a stem cell niche. Since satellite cells reside within basal lamina and sarcolemma, myofibers have been considered as a niche component of muscle stem cells. Although a plethora of studies have suggested that myofibers compose a niche of muscle stem cells, the mechanism of muscle stem cell regulation by myofiber niche is not known.

Puberty is initiated via the hypothalamus-pituitary axis by diffusion of gonadotrophin-releasing hormone from hypothalamus. The increased secretion of gonadotropins such as luteinizing and follicular stimulating hormones primarily acts on the ovary and testis to stimulate production of androgens and estrogens. The function of sex hormones is coordinated by paracrine regulatory mechanisms and essential for establishing and promoting the secondary characteristics of reproductive organs at puberty.

Since the conversion of proliferating juvenile satellite cells into quiescent adult satellite cells occurs during puberty and both androgen receptor, and estrogen receptors α/β are highly expressed in skeletal muscles, the hypothalamic–pituitary–gonadal (HPG) axis might be related to the establishment of satellite cell populations.

In this study, I tested whether the HPG axis is responsible for the conversion of cycling juvenile SCs into quiescent adult SCs at puberty. I investigated how the HPG axis generates quiescent SC pools by activating Notch signaling at puberty. Using mouse genetic models (*Gnrh1*$^{hpg/hpg}$, *MCK-Cre;Ar*$^{f/y}$ (AR$^{\Delta MF}$), *MCK-Cre;Ar*$^{f/y}$*;Esr2*$^{-/-}$, *MCK-Cre;Mib1*$^{f/f}$ (Mib1$^{\Delta MF}$), *Pax7-CreER;Notch1*$^{f/f}$ (N1$^{\Delta SC}$) and *Pax7-CreER;RosaN1* (N1$^{OE/SC}$)), surgical (orchiectomy), and pharmacological (antide treatment) approaches, I revealed a novel mechanism that pubertal sex hormones capacitate myofiber niches to activate Notch signaling in the adjacent

juvenile SCs and to orchestrate the establishment of adult satellite cell populations. Myofibers under impaired HPG axis or myofibers lacking Mib1 fail to send Notch signals to juvenile satellite cells, leading to impaired cell cycle exit and depletion. Moreover, the same axis regulates the re-establishment of quiescent satellite cell populations following injury. These findings reveal an unknown link between the sex hormone and the skeletal muscle, which will provide a new insight to understand why sex hormones should be secreted at puberty and maintained throughout life.

Key word: Adult muscle stem cells (Satellite cells), Myofibers, Sex hormones, Puberty, Notch signaling pathway, Mind-Bomb1 (Mib1)

Student Number: 2009-22929

TABLE OF CONTENTS

LIST OF FIGURES

FIGURES

I. BACKGROUND

1. Myogenesis

Skeletal muscle is a heterogeneous and complicating organ playing multiple functions for survival of the organism. The formation of skeletal muscle myofibers (myogenesis) can be categorized into several distinct phases (Tajbakhsh, 2009). During embryonic myogenesis, mesoderm-derived muscle founder stem cells generate primary muscle fibers serve as templates for further myogenesis (Fig. 1). In subsequent myogenic process, additional fibers are generated along these primary fibers (Parker et al., 2003; Sambasivan and Tajbakhsh, 2007). In the foetal phase, resident myogenic progenitor cells initially proliferate extensively and contribute to myonuclei accretion until puberty (White et al., 2010). As the organism grows, these progenitor cells become

quiescent and reside within basal lamina and sarcolemma as satellite cells. Notably, adult skeletal muscle has remarkable ability to regenerate even after multiple rounds of injury over extended periods (Pellettieri and Sanchez Alvarado, 2007; Schmalbruch and Lewis, 2000). Due to the post-mitotic nature of myofibers, their regeneration in response to muscle damage requires reserve populations of adult muscle stem cells (Lepper et al., 2011). After muscle injury, adult muscle stem cells exit from quiescence and enter into cell cycle to produce a large number of myogenic progenitor cells responsible for the regeneration. Those myogenic progenitor cells differentiate and generate myofibers which can be referred to adult myogenesis.

A number of regulatory molecules are critical for myogenic fate. In embryonic myogenesis, *Pax3* has a critical role in the formation of embryonic muscle fibers that depend on the migration of muscle

progenitor cells from the dermomyotome. *Pax3* also has an essential role in regulating the gene hierarchy which leads to the activation of *MyoD* and the formation of skeletal muscle (Tajbakhsh et al., 1997). Whereas, *Pax7*, a marker of muscle stem cell, is another crucial regulator that plays a critical role postnatally in satellite cells. *Pax7* has been studied for its requirement for the maintenance of muscle stem cells in adult mice and for expansion of muscle stem cells after injury, albeit distinct genetic requirements of *Pax7* between embryonic progenitor cells and adult muscle stem cells has been suggested (Gunther et al., 2013)

Pax3/7 are critical regulators of early lineage specification of muscle stem cell, whereas *Myf5* and *MyoD* commited cells to the myogenic program. Expression of the terminal differentiation genes, required for the fusion of myocytes and the formation of myotubes, are regulated by *myogenin* (*MyoG*) and *MRF4* (Bentzinger et al., 2012).

Figure 1. Embryonic myogenesis

(a,b) Schematic of transverse illustration of the embryo at early **(a)** and late **(b)** stages of somitogenesis. Various domains in the embryo specify the early somite to form the sclerotome and dermomyotome. As the sclerotome segregates, muscle progenitor cells from the dorsomedial lips of the dermomyotome mature to give rise to the myotome. At the level of the limb bud, Pax3-dependent migrating MPCs from the ventrolateral lips give rise to limb muscles.

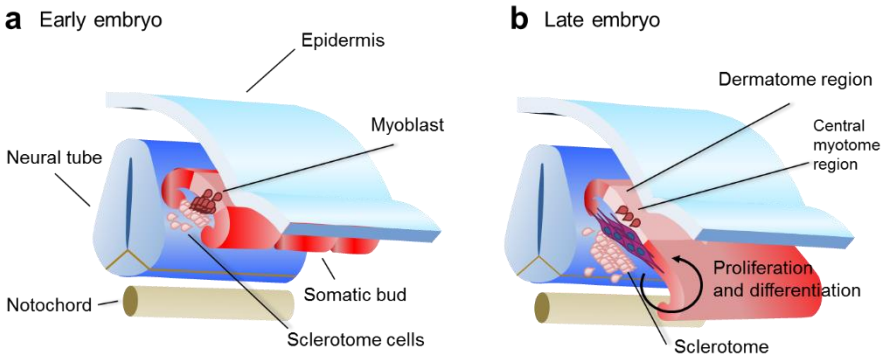
a Early embryo
Epidermis
Myoblast
Neural tube
Somatic bud
Notochord
Sclerotome cells
b Late embryo
Dermatome region
Central
myotome
region
Proliferation
and differentiation
Sclerotome

2. Transcriptional regulation via sex hormones

Sex hormones, androgens and estrogens, conventionally have been defined by their role in reproductive functions and sexual characteristics of organism. Androgens and estrogens, represented by testosterone and 17β-estradiol are produced by leydig cells in the testis and theca cells in the ovary, respectively (Al-Attar et al., 1997; Bhasin et al., 2003).

Androgen and Estrogen signaling through the androgen receptor (AR), and estrogen receptors (ERα and ERβ), a ligand-dependent transcription factor within the steroid receptor superfamily, plays an important role in the development and maintenance of various organs, including bones, and skeletal muscles (Bhasin et al., 2003; Bjornstrom and Sjoberg, 2005; MacLean and Handelsman, 2009; Marino et al., 2006).

Sex hormones can freely diffuse across the plasma membrane. The ability of a cell to respond to a particular hormone depends on the presence of specific receptors for those hormones. Once the hormone binds to its receptor, the receptor is structural and biochemical modified, and it is separated from cytoplasmic chaperone proteins. Thereby it exposes the nuclear localization sequences that results in the activation of the receptor and initiation of the biological actions of the hormone on the target cell (Fig. 2). These receptors then interact with specific binding sites on DNA (hormone response elements (HREs)), thus acting as transcription factors (Wierman, 2007).

Figure 2. Sex hormone pathway

Testosterone (T) is a major androgen simply diffusion and systemically circulating in the blood vessel and. In many tissues, 5-α-reductase converts T into 5-α-dihydrotestosterone (DHT) that more efficiently binds to the androgen receptor. The biological activity of T and DHT occurs through binding to the AR which function as a ligand-dependent transcription factor. Estrogen action in different target tissues is carried out by binding to the estrogen receptors α and β. Estrogen activities are exerted through intracellular receptors that regulate gene expression as a transcription factor after translocation into the nucleus.

The enzymatic reaction of aromatase converts testosterone into 17β-estradiol. The aromatization of testosterone makes available a source of estrogen that stimulate estrogenic functions. The appropriate regulation of sex hormones activity is necessary for developmental, physiological, and pathological processes, particularly male/female sexual development and maturation, as well as the maintenance of target organs.

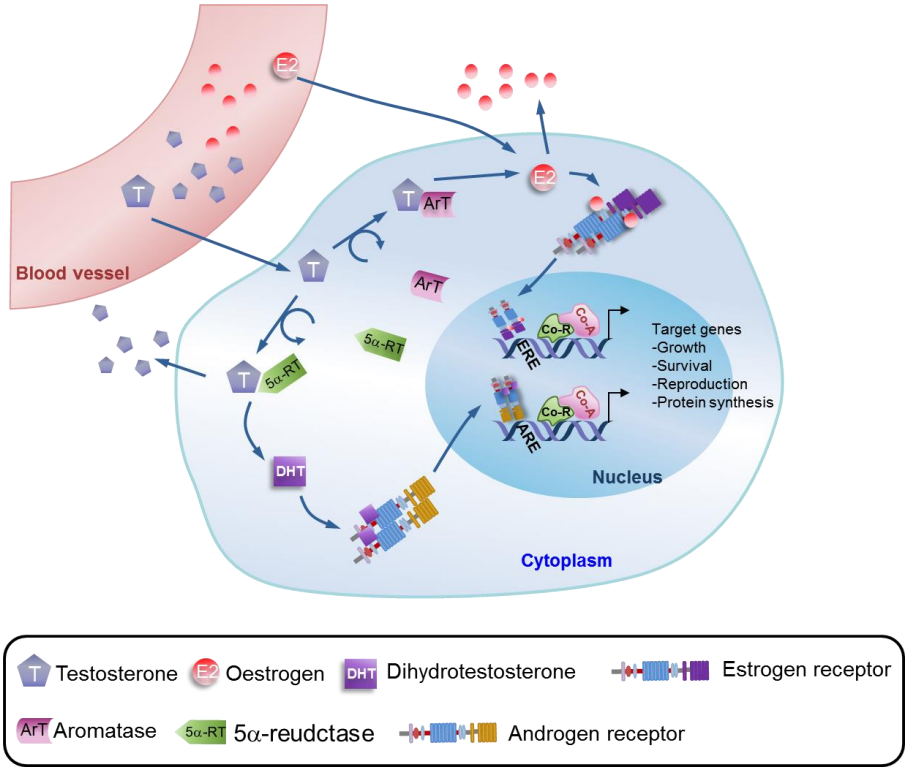
E2
T
Blood vessel
T
ArT
E2
ArT
5α-RT
T
5α-RT
DHT
ERE
Co-R
Co-A
ARE
Co-R
Co-A
Target genes
-Growth
-Survival
-Reproduction
-Protein synthesis
Nucleus
Cytoplasm
T Testosterone
E2 Oestrogen
DHT Dihydrotestosterone
Estrogen receptor
ArT Aromatase
5α-RT 5α-reudctase
Androgen receptor

3. Timing of pubertal onset

Puberty is a complex biologic process involving sexual, physical and psychological development between juvenile and adulthood (Al-Attar et al., 1997; Ebling, 2005; Pinter O., 2007). Timing of puberty is determined by endocrine systems of the Hypothalamic-Pituitary-Gonadal (HPG) axis.

The release of gonadotrophin-releasing hormone (GnRH) from the hypothalamus initiates puberty. GnRH triggers the secretion of gonadotropins such as luteinizing and Follicle-stimulating hormone (LH and FSH) in anterior portion of pituitary glands. Consequently, LH primarily acts on the leydig cells of the testis to stimulate production of androgens, and FSH on the follicular/tubular compartment of ovary to stimulate conversion of estrogen from androgen precursors. Fluctuations of the HPG axis result in changes of the hormones produced by each gland. The production of androgens and estrogens at puberty plays crucial roles for establishing and promoting the

secondary characteristics of reproductive organs which effects locally and also systemically on whole body (Fig. 3)

Figure 3. Hypothalmic-pituitary-gonad (HPG) axis

The GnRH neurons in hypothalamus produces a tropic hormone called GnRH. As GnRH is released, it travels along with the portal vein and binds to secretory cells of the anterior pituitary. Binding of GnRH stimulates pituitary glands to produce luteinizing hormone (LH) and follicle-stimulating hormone (FSH), which are secreted into the bloodstream. Both LH and FSH circulate on blood vessel to produce estrogen in females and testosterone in males. During the puberty, sex hormones promote secondary sex characteristics in peripheral tissues via blood vessel and facilitate sexual or social behaviors by acting on central neural circuits.

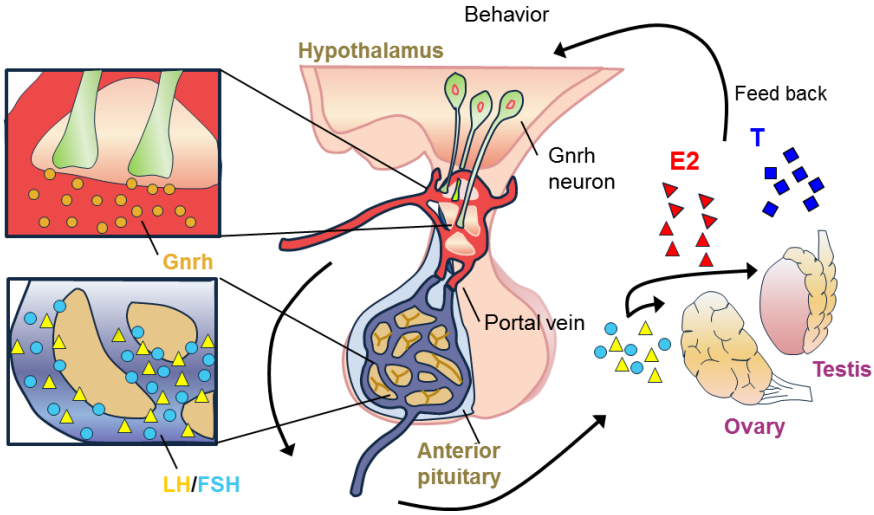
Behavior
Hypothalamus
Feed back
T
E2
Gnrh
neuron
Gnrh
Portal vein
Testis
Ovary
Anterior
pituitary
LH/FSH

4. The Notch signaling pathway

The Notch signaling pathway is an evolutionarily conserved intercellular signaling pathway that is involved in many aspects of development and disease. Notch signaling is a short-range communication between two adjacent cells and can give rise to many downstream responses, including cell fate determination, proliferation, differentiation, apoptosis and tissue-specific gene expression (Fre et al., 2005; Kopan and Ilagan, 2009). The Notch signaling pathway is initiated by the interaction of the four Notch receptors (Notch 1-4) with their ligands such as Delta-like and Jagged in mammals on neighboring cells. Ligand binding leads to two sequential proteolytic cleavages of Notch receptors (S2 and S3 cleavages), and generate soluble Notch intracellular domain (NICD) that trans-locates into the nucleus to regulate transcription complexes containing DNA binding proteins

Su(H)/CBF1/RBP-J/Lag1(CSL). This complex with NICD promotes the transcription of downstream target genes such as Hes and Hey families.

The endocytosis of Notch ligands in the signal-sending cells is absolutely required to Notch signal transduction (Bjornson et al., 2012; Koo et al., 2005; Koo et al., 2007; Song et al., 2008; Song et al., 2006; Weinmaster and Fischer, 2011; Yoon et al., 2008a; Yoon et al., 2008b). Genetic screens in *Drosophila* and Zebrafish identified two class of E3 ubiquitin ligases, *Neuralized* (*Neur*) and Mind Bomb (*Mib*). These E3 ubiquitin ligases have known to conjugate a single ubiquitin protein to Notch ligand and the mono-ubiquitination promote the endocytosis of Notch ligands, which generates the mechanical pulling force necessary for Notch receptor cleavage (Fig. 4). Although all of four E3ubiquitin ligases are implicated in the endocytosis of Notch ligands, only *Mib1* has obligatory role for the Notch signaling in mammalian development but *Neur1*, *Neur2* and *Mib1* are dispensable (Koo et al., 2007).

Figure 4. The Notch signaling pathway

The Notch receptor is activated by binding to a ligand presented by a neighboring cell. Endocytosis and membrane trafficking regulate ligand and receptor availability at the cell surface. Ligand endocytosis is also thought to generate mechanical force to promote a conformational change in the bound Notch receptor. This conformational change exposes site 2 (S2) in Notch for cleavage by ADAM metalloproteases. γ-Secretase cleavage (S3/S4) can generate NICD by cleaving Notch receptor and then NICD enters the nucleus where it associates with the DNA-binding protein CSL (CBF1/RBPjκ/Su(H)/Lag-1). In the absence of NICD, CSL may associate with ubiquitous corepressor (Co-R) proteins and histone deacetylases (HDACs) to repress transcription of some target genes.

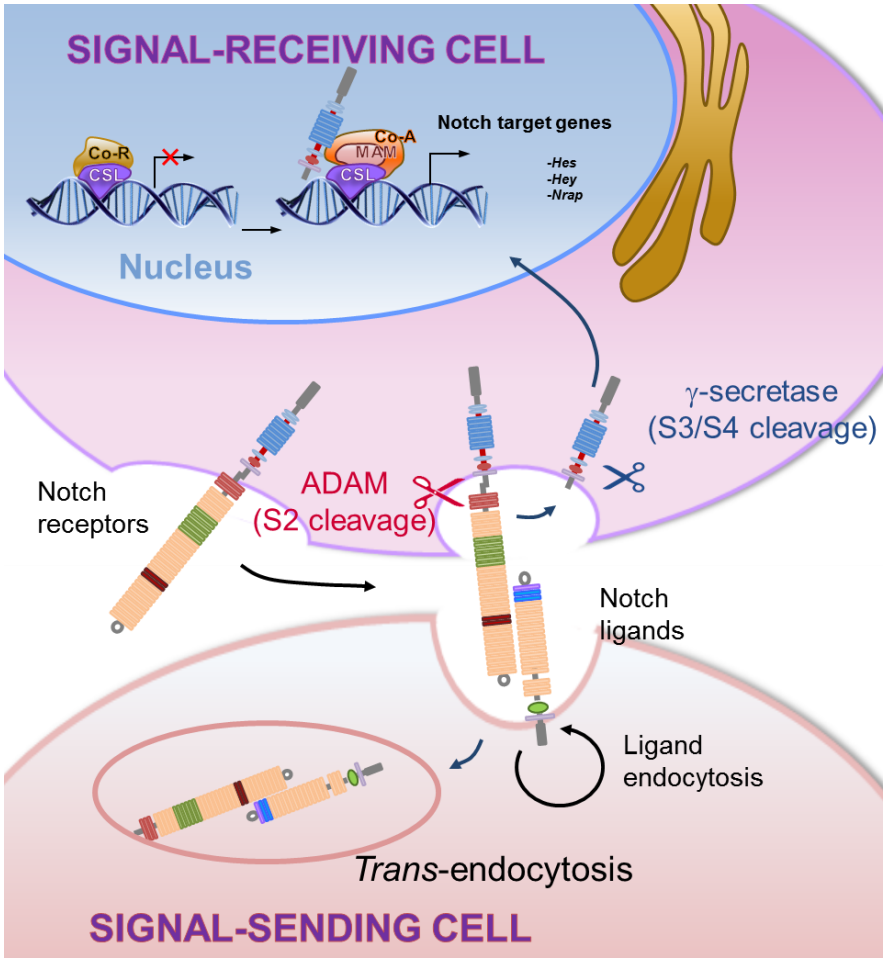
SIGNAL-RECEIVING CELL
Co-R
CSL
Co-A
MAM
CSL
Notch target genes
-Hes
-Hey
-Nrap
Nucleus
γ-secretase
(S3/S4 cleavage)
Notch
receptors
ADAM
(S2 cleavage)
Notch
ligands
Ligand
endocytosis
Trans-endocytosis
SIGNAL-SENDING CELL

II. INTRODUCTION

Skeletal muscles develop from the consecutive progression of multipotent stem/myogenic progenitors that enter the myogenic program. These stem/progenitors which possess distinct characteristics, contribute to myogenic differentiation into myofibers during embryonic, fetal, and postnatal myogenesis (Tajbakhsh, 2009). During postnatal myogenesis, the resident stem/myogenic progenitors proliferate extensively for myonuclear accretion into pre-existing muscle fibers (Schultz, 1996; White et al., 2010). As the organism grows, however, the population of proliferating stem/myogenic progenitors decreases, and the number of myonuclei in muscle fibers reaches a steady state (White et al., 2010). Eventually, the stem/myogenic progenitors known as juvenile satellite cells (SCs) enter quiescence until they meet a stimulation signal. (Davis and Fiorotto,

2009; Gibson and Schultz, 1983). In fact, the number of cycling $Pax7^+$ SCs declines during postnatal growth, whereas that of quiescent $Pax7^+$ SCs increases (Tajbakhsh, 2009; White et al., 2010), suggesting that some of the cycling $Pax7^+$ SCs exit the cell cycle and contribute to the establishment of adult SC populations, and that sex hormones might be involved in these processes. However, the molecular mechanism that is responsible for converting highly "proliferating juvenile" SCs into "quiescent adult" SCs remains unclear, although the reserve pool of quiescent $Pax7^+$ SCs is essential for skeletal muscle regeneration throughout life (Gunther et al., 2013; Sambasivan et al., 2011).

Sex hormones (androgens and estrogens) are essential for establishing and promoting the secondary characteristics of reproductive organs at puberty, and also play important roles in various organs, including

bones, and skeletal muscles (Wierman, 2007). Since both androgen receptor (AR) and estrogen receptors (ERs) α/β are highly expressed in skeletal muscles (Kalbe et al., 2007; Sinha-Hikim et al., 2004), these sex hormones may play an important role in the skeletal muscle development after puberty. Although a plethora of studies have suggested that androgens and estrogens are implicated in muscle growth and regeneration (Brown et al., 2009; Chambon et al., 2010; Velders et al., 2012), the mechanism underlying the regulation of skeletal muscle integrity by these sex hormones is poorly understood.

The Notch signaling pathway is an evolutionarily conserved intercellular signaling mechanism that has been implicated in stem cell maintenance and cell fate decision in a variety of tissues including skeletal muscles (Conboy and Rando, 2002; Fre et al., 2005; Song et

al., 2008; Yoon et al., 2008a). Through cell-cell communications, the Notch signaling is initiated by E3 ubiquitin ligases [Mind bomb-1 (Mib1), Mib2, Neuralized-1 (Neur1), and Neur2], which trigger endocytosis of Notch ligands [Deltalike-1 (Dll1), Dll4, Jagged-1 (Jag1) and Jag2] that interact with Notch receptors (Notch1-4) leading to sequential cleavage of Notch receptors (Kopan and Ilagan, 2009). Once cleaved, Notch intracellular domain (NICD) translocates into the nucleus and interacts with Rbpj-κ consequently activating Notch target genes. Notch signaling has critical roles in skeletal muscle development, such as myogenic differentiation of the multipotent cells in the dorsal dermomyotome (Rios et al., 2011), maintenance of muscle progenitors during fetal myogenesis (Mourikis et al., 2012a; Schuster-Gossler et al., 2007; Vasyutina et al., 2007), homing of SCs (Brohl et al., 2012), maintenance of quiescent SCs in adult (Bjornson et al., 2012; Mourikis

et al., 2012b), and proliferation of SCs during regeneration (Brack et al., 2008; Conboy and Rando, 2002). Although it is clear that Notch signaling plays a critical role in the maintenance of SC stemness, distinct functions of Notch signaling in various contexts still remain to be determined.

Puberty is initiated via the hypothalamus-pituitary (HP) axis by secreting GnRH (Ebling, 2005) and the conversion of proliferating juvenile SCs into quiescent adult SCs occurs during puberty. Thus, I tested whether the HPG axis is responsible for the conversion of cycling juvenile SCs into quiescent adult SCs at puberty. Consequently, I investigated how the HPG axis generates quiescent SC pools by activating Notch signaling at puberty and found a missing link between the HPG axis and the establishment of adult SC populations at puberty.

III. MATERIALS AND METHODS

1. Mice

The male mice were used in this study. *Mib1*$^{f/f}$ and *Ar*$^{f/y}$ mice were previously described(Koo et al., 2007; Shiina et al., 2006). *Rosa-Notch1* mice were kindly provided by D. Melton (Harvard Stem Cell Institute, Harvard University, Boston, MA, USA)(Murtaugh et al., 2003). *MCK-Cre*, *Pax7-Cre*^{ER}, *Notch1*$^{f/f}$, *Esr2*$^{-/-}$, *Gnrh1*$^{hpg/hpg}$ transgenic, and knockout mice were purchased from The Jackson Laboratory (Bar Harbor, ME, USA). Mice carrying the *Mib1* gene (*Mib1*$^{f/f}$), the *Ar* gene (*Ar*$^{f/y}$), and the *Notch1* gene flanked by a pair of *loxP* sites (*Notch1*$^{f/f}$) were used for myofiber (MF)- or satellite cell (SC)-specific deletion studies. *Rosa-Notch1* mice harbor the intracellular domain of mouse Notch1 in the ubiquitously expressed

Rosa26 locus, the expression of which is blocked in the absence of *Cre*. *Rosa-Notch1* mice were crossed with *Pax7-Cre*^{ER} mice. Nicd and nuclear GFP proteins were expressed in Pax7^{+} cells upon tamoxifen injection. Tamoxifen (5 mg/ml in corn oil) (Sigma-Aldrich, St. Louis, MO, USA) was intraperitoneally (i.p.) administered daily for 3 days (100 mg/kg body weight). All of these mouse lines were backcrossed onto a C57BL/6 background and were housed and handled according to the guidelines of the ethical committees at Seoul National University. The abbreviation ΔMF, ΔSC, N1$^{OE/SC}$ indicates *MCK-Cre* (myofiber-specific knockout mouse), *Pax7-Cre*^{ER} (satellite cell-specific inducible knockout mouse), and *Pax7-Cre*^{ER}*;Rosa-N1icd* (satellite cell-specific inducible overexpression mouse), respectively. Abbreviations: Mib1^{WT} (*MCK-Cre*); Mib1$^{\Delta MF}$ (*MCK-Mib1*$^{f/f}$); N1^{WT} (*Pax7-Cre*^{ER}); N1$^{\Delta SC}$ (*Pax7-Cre*^{ER}*;N1*$^{f/f}$); N1$^{OE/SC}$ (*Pax7-Cre*^{ER}*;Rosa-N1icd*); N1^{WT} (*N1*$^{f/f}$);

Ar^{WT} (*MCK-Cre*); $Ar^{\Delta MF}$ (*MCK-Ar$^{f/y}$*); and $Ar^{\Delta MF}$;$Esr2^{-/-}$ (*MCK-Ar$^{f/y}$; Esr2$^{-/-}$*) Controls are designated as the WT of comparing mutant mice.

2. Myogenic cell (MC) and SC isolation

MC isolation was performed according to previously demonstrated protocol (Ohkawa et al., 2012) with modifications. Dissected hindlimb skeletal muscles were digested in collagenase type II (100 units/ml) in PBS supplemented with 1 mM $CaCl_2$ without mincing at 37°C for 60 min. Following collagenase treatment, the monocytes and debris (Fraction A) were separated from the digested mixture by a 70-μm nylon membrane cell strainer (BD Biosciences, Medford, MA, USA). The remainders were further digested with dispase (5–10 mg/ml) for 30 min, and myogenic cells (MC, Fraction B) were separated from MFs by passing through a 40-μm nylon cell strainer (BD Biosciences). In

order to verify the isolated fractions, FACS, qRT-PCR, and immunocytochemistry (ICC) were performed.

SC isolation was performed according to a previously reported protocol(Liu et al., 2013; Liu et al., 2015). Hindlimb muscles [*tibialis anterior* (TA), *gastrocnemius* (GA), *extensor digitorum longus* (EDL), and *soleus*] were mechanically dissected and dissociated in Dulbecco's modified Eagle's medium (DMEM) containing 10% horse serum (Hyclone, Logan, UT, USA) and collagenase II (500 units/ml; Invitrogen, Carlsbad, CA, USA) at 37°C for 90 min and were further digested in dispase (10 mg/ml; StemCell Technologies, Vancouver, BC, Canada) for 60 min. These digested suspensions were subsequently triturated and washed with DMEM to harvest mononuclear cells. Mononuclear cells were stained with Sca1-FITC (clone D7; BioLegend,

San Diego, CA, USA), TER119 (clone TER-119; BioLegend), CD31-APC (clone MEC 13.3; BD Biosciences), CD45-APC (clone 30-F11; BD Biosciences), and Vcam1-Biotin (clone 429; BD Biosciences). Streptavidin-PE (BD Biosciences) was used as a secondary reagent. Stained cells were analyzed and $Vcam^{+}Sca1^{-}$ SCs were isolated using a FACS Aria II cell sorter (BD Biosciences). SC-isolated populations were further verified by qRT PCR and ICC using SC-specific (*Pax7* and *Itgα7*) and MF-specific (*Mck* and *MyHC1*) markers.

3. MF isolation from EDL muscles

For myonuclei quantification and *in vitro* culture, MFs were carefully isolated from EDL muscles. Dissected EDL muscles were subjected to enzymatic digestion with collagenase I (2 mg/ml, Gibco Invitrogen, Grand Island, NY) for 80 min at 37°C. Subsequently, the digested EDL

muscles were blocked in DMEM and 10% horse serum (Gibco). Next, single MFs were gently released from the muscles. Undamaged and non-contracted fibers were transferred into a new dish containing fresh medium. Isolated MFs were maintained at 37°C in a 5% CO_2 cell incubator between each wash cycle.

4. MC and MF culture

For MC and MF cultures, isolated MCs or MFs were incubated in DMEM containing 20% hormone free FBS and 0.5% chick embryo extract (Sigma-Aldrich). These MCs or MFs were subsequently treated with ethanol (Sigma-Aldrich), 5α-dihydrotestosterone-17β-ol-3-one C-IIIN (DHT, A8380; Sigma-Aldrich, 100 nM), or 17β-estradiol (E2, E8875; Sigma-Aldrich, 100 nM). For the inhibitor study, freshly isolated MFs were incubated with E2 and a selective antagonist to ERα,

1,3-bis(4-hydroxyphenyl)-4-methyl-5-[4-(2-piperidinylethoxy)phenol]-1H-pyrazole dihydrochloride (MPP) or E2 and selective antagonist to ERβ, 4-(2-phenyl-5,7-bis(trifluoromethyl)pyrazolo[1,5-a]pyrimidin-3-yl)phenol (PHTPP) for 24 h.

5. RNA isolation and RT-qPCR

Total RNA was extracted from the freshly isolated EDLs, TA muscles, or MFs using an RNeasy Micro Kit (Qiagen, GmbH, Hilden, Germany) or TRI Reagent (Sigma-Aldrich) and analyzed by RT-qPCR. First-strand complementary DNA was synthesized from 1 μg of RNA using Promega's RT system (Promega, Madison, WI, USA). RT-qPCR was performed via quantitative real-time RT-PCR (Qiagen) with SYBR Green technology (SYBR Premix Ex Taq, Qiagen) using primers

against using specific primers (Primer sequences are described in Supplementary Table. 4). The thermocycling conditions were as follows: initial step of 10 min at 95°C, followed by 50 cycles of denaturation for 15 s at 94°C, annealing for 10 s at 60°C, and extension for 15 s at 72°C. The reactions were run in triplicate, and the automatically detected threshold cycle (Ct) values were compared between samples. Relative quantification of gene expression was performed using the delta delta Ct method. Transcripts of the *β-actin*, *Gapdh*, or *18s rRNA* housekeeping genes were used as endogenous controls.

6. Muscle injury

For $BaCl_2$ injury, mice were anesthetized with 2% Avertin (0.02 ml/g body weight) and injected with 50 μl $BaCl_2$ (1.2%; Sigma-Aldrich) in

the TA muscles. For cell proliferation analysis, BrdU was administered intraperitoneally at 5 μg/g body weight. The mice were sacrificed 2 h after BrdU injection. The TA muscles were dissected, frozen in Optimal Cutting Temperature (OCT) compound (SAKURA, Torrance, CA, USA), cooled with liquid nitrogen, and stored at −80°C until analysis. Seven-μm sections were collected from TA muscles and stained with hematoxylin and eosin (H&E).

7. Sex hormone administration and measurement of hormone levels

Ten-day-old male mice were subcutaneously (s.c.) injected with corn oil (Veh), DHT (10 μg/g body weight in corn oil), or E2 (0.5 μg/g body weight in corn oil). Hindlimb muscles were removed 3 days after hormone administration, frozen in liquid nitrogen, and stored at −80°C

until the assay could be performed. To measure circulating hormone levels, serum samples were taken from each group and analyzed by ELISA to evaluate the concentration of testosterone using commercially available kits (R&D Systems, Abingdon, UK), according to the supplier's instructions. To measure E2, a radioimmunoassay (RIA) kit (Beckman Coulter, Pasadena, CA, USA) was used according to the supplier's instructions. To prepare serum, whole blood was collected from the eyes and placed into 1.5-ml Eppendorf tubes. The blood was clotted by incubating at room temperature for 30 min, and the serum was collected after centrifugation for 10 min at 4,000 rpm and stored at −80°C until the assay.

8. Measurement of E2 hormone levels using LC-MS/MS

The reference materials of E2 and 2,4,16,16-d_4-E2 (d_4-E2; isotopic

purity ≥ 98%) as an internal standard were purchased from Steraloids (Newport, RI, USA) and C/D/N isotope (Pointe-Claire, Quebec, Canada), respectively. For solid-phase extraction (SPE), an Oasis HLB cartridge (3 ml, 60 mg) was obtained from Waters (Milford, MA, USA). The chemical derivatization reagents, dansyl chloride and pentafluoropropionic anhydride (PFPA) were acquired from Sigma (St. Louis, MO, USA). For preparing calibration samples, the commercially available steroid-free serum was obtained from Scipac (Sittingbourne, UK).

The instrumental conditions are described as follows: Serum E2 was determined using an UltraLC 100-XL (AB Sciex; Framingham, MS, USA) coupled to QTRAP 6500 mass spectrometer (AB Sciex). Chromatographic separations were performed on a 3 μm particle

Hypersil Gold-C18 column (150 × 2.1 mm; Thermo Scientific; Waltham, MA, USA) at a flow rate of 0.3 ml/min. The MS parameters were as follows: spray voltage, 5500 V; interface heater temperature, 150°C; collision gas, nitrogen at 60 psi; source temperature, 650°C; Q1 and Q3 peak widths (FWHM), 0.4 u and 0.7 u. To minimize run-to-run variations in quantitative analysis, the isotope-dilution mass spectrometry (IDMS), which is the primary method with an adjusted isotope labeled standard(Van Uytfanghe et al., 2004), was conducted. Both E2 and d_4-E2, as their dansyl-PFP derivatives, were detected in the electrospray positive ionization of the selected-reaction monitoring (SRM) mode with *m/z* 652.2 $[M+H]^+$→ *m/z* 156.0 and *m/z* 656.2 $[M+H]^+$→ *m/z* 171.1, respectively. The data acquisition and analysis were performed using the Analyst software (ver. 1.6.2; AB Sciex).

For sample preparation, the selective extraction of serum E2 was based on previous reports(Moon et al., 2011; Xu et al., 2007). In brief, 40-100 μl of mouse serum samples were spiked with 20 μl of d_4-E2 at 0.5 ng/ml. The samples were diluted with 2.9 ml of 0.2 M sodium acetate buffer (pH 5.2) and vortexed for 30 s. The SPE cartridges were preconditioned with 2 ml of methanol followed by 2 ml of deionized water. After loading the sample onto the Oasis HLB cartridge, it was washed with 2 ml water and eluted twice with methanol (2 ml). The combined methanol was evaporated under a nitrogen stream at 40°C. The dried extracts were added with 50 μl of 0.1 M sodium carbonate-bicarbonate buffer (pH 9) and then derivatized with 100 μl of dansyl chloride (1 mg/ml in acetone) for 10 min at 60°C. The reaction mixture was evaporated in a nitrogen stream and dried in a vacuum desiccators over P_2O_5-KOH for at least 30 min. Finally, the dried residue was

subsequently derivatized with 20 μl of PFPA in 100 μl acetone at 50°C for 30 min, and evaporated. The resulting mixture was reconstituted with 100 μl of methanol and then an aliquot (10 μl) was injected into the LC-MS/MS system. The devised two-step derivatization method produced 3-dansyl-17β-PFP E2 and improved chromatographic properties with the lower limit of quantification (LLOQ) at 5 pg/ml, which was defined as the lowest concentration with accuracy and precision of less than 20%.

9. Immunoblot analysis

Muscle tissues, MFs, MCs, or SCs were homogenized in 1 ml RIPA buffer (50 mM Tris-HCl, pH 7.5, 0.5% SDS, 20 μg/ml aprotinin, 20 μg/ml leupeptin, 10 μg/ml phenylmethylsulfonyl fluoride, 1 mM sodium orthovanadate, 10 mM sodium pyrophosphate, 10 mM sodium

fluoride, and 1 mM dithiothreitol). Bradford's reagent (Bio-Rad Laboratories, Hercules, CA, USA) was used for estimating total protein concentrations. Total proteins were analyzed by electrophoresis in 8%–15% polyacrylamide gels and transferred to PVDF membranes (Millipore, Overijse, Belgium). The membranes were incubated with primary antibodies overnight at 4°C. After incubation with the corresponding HRP-conjugated secondary antibodies (Sigma-Aldrich or Invitrogen), the membranes were developed using the LAS imaging system (Fujifilm, Tokyo, Japan). GAPDH, β-tubulin, or β-actin was used as a loading control.

10. Antide administration and Orchiectomy

One-week-old littermate mice were s.c. injected with Nal-Lys gonadotropin releasing-hormone antagonist (Antide) (bioWorld,

Dublin, OH, USA) at a dose of 3.0 mg/kg body weight weekly for 4 weeks. Antide was dissolved in 20% propylene glycol and 0.9% saline. Two-week-old male mice were anesthetized with 2% Avertin (0.02 ml/g body weight) and orchiectomized(Roubinian et al., 1978).

11. Immunofluorescence of muscle sections

Seven-μm sections were collected from the hindlimb muscles and immunostained. Immunohistochemistry on muscle cryosections was performed using the following steps: 7-μm sections were fixed in 4% paraformaldehyde for 10 min, washed in PBS, and treated in MOM blocking solution, according to the manufacturer's instructions (FMK-2201; Vector Laboratories, Burlingame, CA, USA). The sections were incubated with primary antibodies overnight at 4°C after blocking for 1 h at room temperature with 5% bovine serum albumin in PBS. The

slides were washed with PBS several times and incubated with the appropriate secondary antibodies for 1 h at room temperature. The slides were counterstained with Hoechst and mounted with Vectashield (H-1000; Vector Laboratories, Burlingame, CA, USA) after washing with PBS. Cells merge with Hoechst signal are counted and quantified for statistical analyses.

12. EdU labeling

On days 14 and 21 after 1.2% $BaCl_2$ injury in TA muscles, mice were i.p. injected with EdU (100 μg/mice) one hour before sacrifice. To detect proliferating cells, Click-iT™ EdU Cell Proliferation Assay Kit (C10337, Invitrogen, Carlsbad, CA, USA) was used. For EdU staining, cryosections were fixed in 4% PFA for 10 minutes at room temperature, washed with 3% BSA for twice, and treated with 0.5% Triton™ X-100

(T9284, Sigma, St. Louis, MO, USA) permeabilization buffer for 15 minutes at room temperature followed by 3% BSA washing. The sections were treated with Click-iT™ reaction cocktail for 30 minutes at room temperature in dark followed by 3% BSA washing. After incubation with desired primary/secondary antibody, the slides were mounted with Vectashield (H-1200, Vector laboratories, Burlingame, CA, USA).

13. DNA construct and luciferase assay

A 5,000-bp genomic fragment of the *Mib1* promoter was cloned from the BAC clone of the mouse genomic DNA using the 5′ primer CCCCATGAGGGCAGAAACCAT and the 3′ primer TTATGATGCAACAAATATAT. The fragment was inserted into the pGL4.3 luciferase reporter plasmid (Promega) to generate the WT-

Mib1 promoter plasmid. To generate the promoter mutant construct, 3 point mutations were introduced into the WT-*Mib1* plasmid by using a site directed mutagenesis kit (Stratagene, La Jolla, CA, USA).

Luciferase assays were performed by seeding 1×10^6 C2C12 cells per well in 6-well dishes. Cells were transfected with 5 μg of luciferase plasmid constructs (WT, ERE-MT, ARE-MT, dMT) and 50 ng of the *LacZ* control vector. Cells were transfected using polyethylenimine (PEI; Bioscience), according to the manufacturer's instructions. After 24 h of transfection and treatment, the cells were lysed, and luciferase and β-galactosidase activities were measured using a Turner BioSystems luminometer (Promega).

14. Microarray and IPA

RNA isolation from TA muscles was performed with the TRI reagent (Sigma) following the manufacturer's guide. Processing of the RNA and hybridization to whole muscle transcriptomes were analyzed using Illumina Bead Chip Mouse Ref8-v2 arrays containing 25,600 well-annotated RefSeq transcripts. Gene expression values were normalized with quantile normalization across all samples and log2 transformed. The microarray datasets have been deposited to Gene Expression Omnibus database [GSE64454]. IPA tools were used to conduct a bioinformatics evaluation of DHT responding gene candidates. Details and technical requirements are available from the IPA Website (www.ingenuity.com). A graphical representation shows the IPA-generated hypothetical networks based on the molecular relationships, interactions, and pathway associations.

15. Statistical and Reproducibility

All statistical analyses were performed using GraphPad Prism 5 (GraphPadSoftware) and Statistical Package for the Social Sciences (SPSS, IBM Corporation). Unless otherwise noted, all the error bars represent the SD. Data were analyzed using two sample *t*-test (for a difference in mean), *F*-test (for variance test), Bootstrap test with 10,000 replications (for relatively small sample size), ANOVA (for comparison of significant difference in means among groups), Tukey's pairwise comparison test (after applying ANOVA for multi-group comparison), Poisson generalized linear model (GLM) (for countable data), Pearson's χ^2 test (for countable independent data) and Kruskal-Wallis test (for continuous data without normality) according to data. A p value of < 0.05 considered statistically significant at the 95% confidence level. At least, independent experiments are performed in

triplicate.

16. Optical systems

Immunofluorescence was performed using a Zeiss Observer Z1 fluorescent microscope (Zeiss, Oberkochen, Germany) equipped with a SPOT Flex camera or a Zeiss confocal system LSM710. For myofiber diameter measurements, morphometric software (INS Industry, Seoul, Korea), spot software (version 5.1, Diagnostic Instruments, Sterling Heights, MI, USA) and Photoshop CS6 (Adobe) were used.

IV. RESULTS

Notch signaling is activated in juvenile SCs at puberty

Since sex hormones increase dramatically at puberty (Ober et al., 2008; Safranski et al., 1993), I hypothesized that sex hormones are responsible for the conversion of cycling juvenile SCs into quiescent SCs. When I injected DHT into 10-day-old pre-pubertal mice, most $Pax7^+$ cells in the *tibialis anterior* (TA) muscles became $Ki67^-p57^+$ 3 days after DHT treatment, whereas remained $Ki67^+p57^-$ in the control (Veh) (Fig. 5a, c and d). Additionally, proliferating $MyoD^+$ cells disappeared after DHT treatment but were maintained in controls (Fig 5e). Microarray analysis revealed that the expression of 79 potential cycling SC-marker genes decreased in TA muscles after DHT treatment, while 72 potential quiescent SC-marker genes increased (Fukada et al.,

2007; Liu et al., 2013) (Fig. 6a). Pathway analysis revealed that DHT treatment induced the expression of Notch signaling components, including Notch target genes (*Hes1*, *Hey1*, and *HeyL*) and an E3 ubiquitin ligase, *Mib1* (Koo et al., 2007) (Fig. 6b and c), which were confirmed by qRT-PCR (Fig. 5b).

Immunohistochemical analysis showed that Nicd in $Pax7^+$ cells was detected in 3-week-old TA muscles, while almost undetectable in 2-week-old (Fig. 7 b and c). Interestingly, most $Pax7^+Nicd^-$ cells were $BrdU^+$, whereas most $Pax7^+Nicd^+$ cells were $BrdU^-$ (Fig. 8). The number of $Pax7^+Nicd^+$ cells and Notch target genes gradually increased with age, whereas that of $Pax7^+Nicd^-$ cells progressively decreased (Fig. 7), suggesting that Notch activation may be implicated in the conversion of cycling $Pax7^+Nicd^-$ juvenile SCs into quiescent

$Pax7^{+}Nicd^{+}$ SCs. To test this possibility, I crossed satellite cell-specific inducible *Pax7-Cre*^{ER} ($N1^{WT}$) transgenic mice(Lepper and Fan, 2010) with *Notch1*$^{f/f}$ (Yang et al., 2004) (*Pax7-Cre*^{ER}*; Notch1*$^{f/f}$, hereafter $N1^{\Delta SC}$) and *Rosa-N1icd* over-expressed mice(Murtaugh et al., 2003) (*Pax7-Cre*^{ER}*;Rosa-N1icd,* hereafter $N1^{OE/SC}$), and injected tamoxifen into 7-day-old pre-pubertal mice. Intriguingly, most $Pax7^{+}$ cells were proliferating ($Ki67^{+}BrdU^{+}$) in 4-week-old $N1^{\Delta SC}$ TA muscles, but mostly quiescent ($Ki67^{-}BrdU^{-}$) in $N1^{WT}$ TA muscles (Fig. 9). Consistently, the expressions of the cell cycle inhibitors *p21*, *p27*, and *p57,* and the quiescent SC markers, *Sprouty-1* (*Spry1*) and *Calcitonin receptor* (*Calcr*) (Chakkalakal et al., 2012; Fukada et al., 2007), significantly decreased in SCs isolated from $N1^{\Delta SC}$ mice compared to those in controls, while the expressions of *MyoD* and *Myogenin* (*MyoG*) increased (Fig. 10), suggesting premature differentiation of cycling SCs

in $N1^{\Delta SC}$ mice. Indeed, $Pax7^{+}$ cells disappeared in 8-week-old $N1^{\Delta SC}$ mice (Fig. 11). In contrast, most $Pax7^{+}$ cells became quiescent in $N1^{OE/SC}$ mice 3 days after tamoxifen injection, whereas they continued to proliferate in $N1^{WT}$ mice (Fig. 12 and 13). Together, these results indicate that sex hormones drive the conversion of cycling juvenile SCs into quiescent SCs by activating Notch signaling at puberty.

$Mib1^{+}$ myofibers convert juvenile SCs into quiescent SCs

To investigate how Notch signaling is activated in cycling juvenile SCs, I separated the myogenic mononuclear cells (MCs) and MFs from 4-week-old TA muscles. Notably, Delta like-1 (Dll1) and Jagged-1 (Jag1) were expressed in MFs, whereas Nicd and Hes5 in MCs (Fig. 14a). Intriguingly, the expression of Mib1 dramatically increased in MFs of 3-week-old mice (Fig. 14b), correlating with the generation of

Nicd in MCs (Fig. 8) and $Pax7^+$ cells (Fig. 9). Since Mib1 in the signal-sending cells plays an obligatory role in Jag- as well as Dll-mediated Notch activation(Jeong et al., 2009; Jeong et al., 2012; Kim et al., 2008; Koo et al., 2005; Koo et al., 2007; Song et al., 2008; Yoon et al., 2008a; Yoon et al., 2008b) I specifically ablated the *Mib1* gene in the MFs by crossing myofiber-specific *muscle creatinine kinase (MCK)-Cre* transgenic mice(Bruning et al., 1998; Camarda et al., 2004) with $Mib1^{f/f}$ mice(Koo et al., 2007) to generate *MCK-Cre;*$Mib1^{f/f}$ (hereafter, $Mib1^{\Delta MF}$) mice (Fig. 15). In $Mib1^{\Delta MF}$ mice, Nicd and Hes5 were not expressed in MCs and SCs (Fig. 16a). Moreover, most $Pax7^+$ SCs were $Nicd^-$ in 4-week-old $Mib1^{\Delta MF}$ TA muscles (Fig. 16b, c). Taken together, these results show that Notch activation in $Pax7^+$ juvenile SCs requires the expression of Mib1 in MFs.

Histological analysis showed that the number of sublaminar myonuclei and the cross-sectional area of the MFs in Mib1$^{\Delta MF}$ mice were comparable to controls (Supplementary Fig. 3c, d). However, the expression levels of *p21, p27,* and *Spry1* did not increase in Mib1$^{\Delta MF}$ TA muscles, whereas the levels gradually increased in *MCK-Cre* (Mib1^{WT}) TA muscles along ages (Fig. 17). Moreover, the expression of *MyoD/MyoG* increased in SCs from Mib1$^{\Delta MF}$ hindlimb muscles compared to that from Mib1^{WT} hindlimb muscles (Fig. 18). Immunohistochemical analysis showed that Pax7^{+}MyoD^{+}/MyoG^{+} cells increased in Mib1$^{\Delta MF}$ TA muscles (Fig. 19 and 20), suggesting precocious differentiation of cycling SCs. Indeed, most Pax7^{+} cells in Mib1$^{\Delta MF}$ TA muscles, even in 8-week-old, were still cycling and eventually became undetectable in 12-week-old mice, whereas Pax7^{+}Ki67^{+} cells gradually decreased in the control and subsequently

became $Pax7^{+}Ki67^{-}$ (Fig. 21). Additionally, $Lin^{-}Vcam\text{-}1^{+}Sca\text{-}1^{-}$ cells dramatically decreased in 8-week-old $Mib1^{\Delta MF}$ and $N1^{\Delta SC}$ hindlimb muscles compared with control (Fig. 22). When I injected $BaCl_2$ into the TA muscles of 8-week-old mice, regenerative myogenesis was completely abrogated in $Mib1^{\Delta MF}$ mice (Fig. 23). Similar results were also observed in a cold injury experiment(Brack et al., 2008) (not shown). Neither DHT nor E2 treatement could convert juvenile SCs into quiescent SCs in $Mib1^{\Delta MF}$ mice (Data not shown). These data show that the conversion of cycling $Pax7^{+}$ juvenile SCs into $Pax7^{+}$ quiescent adult SCs requires Mib1 expression in the MFs at puberty.

Sex hormones induce Mib1 expression in myofibers by AR and ERβ pathways

Bioinformatics analyses revealed putative AR- and ER-binding sites

at positions −244 and −1559, respectively, in the mouse *Mib1* promoter. Indeed, DHT and E2 induced luciferase activity in the wild-type construct (Veh:1, DHT: 3.84 and E2: 2.54 fold) but failed to do so in the corresponding mutants of the AR- and ER-binding sites (Veh: 1, DHT: 0.89 and E2: 1.21 fold) (Fig. 24a). When I cultured freshly isolated MFs from the *extensor digitorum longus* muscles of 10-day-old mice treated with either DHT or E2, both DHT and E2 can readily induced Mib1 expression in an additive manner (Fig. 24b). Since both ERα and ERβ are highly expressed in skeletal muscles(Kalbe et al., 2007; Wiik et al., 2009), I investigated which ER is responsible for the induction of Mib1 in MFs by using myofiber-specific *Ar*-ablated (*MCK-Cre;Ar*$^{f/y}$(Shiina et al., 2006); hereafter, Ar$^{\Delta MF}$) mice (Supplementary Fig. 6a-e). The induction of Mib1 in MFs from Ar$^{\Delta MF}$ mice was inhibited by a selective antagonist of ERβ, 4-(2-phenyl-5,7-

bis(trifluoromethyl)-pyrazolo[1,5-a]pyrimidin-3-yl)-phenol (PHTPP)(Weiser et al., 2009) , but not by a selective antagonist of ERα, 1,3-Bis(4-hydroxyphenyl)-4-methyl-5-[4-(2-piperidinylethoxy)phenol]-1H-pyrazole-dihydrochloride (MPP)(Sun et al., 2002) (Fig. 25a, b). To confirm that the induction of Mib1 in MFs relies on AR and ERβ signaling, I generated *MCK-Ar$^{f/y}$Esr2$^{-/-}$* ($Ar^{\Delta MF}Esr2^{-/-}$) mice*(Shiina et al., 2006; Velders et al., 2012)* (Fig. 28). Importantly, DHT and E2 induced Mib1 expression in MFs from 4-week-old $Esr2^{-/-}$ and $Ar^{\Delta MF}$ mice, respectively, when cultured, whereas neither DHT nor E2 induced Mib1 expression in $Ar^{\Delta MF}Esr2^{-/-}$ MFs (Fig. 25c), showing that DHT and E2 can independently induce Mib1 expression in MFs.

As AR and ERβ are expressed in both MCs and MFs (Carson et al., 2002; Doumit et al., 1996; Kadi et al., 2000; Sinha-Hikim et al., 2004),

the isolated MCs and MFs were cultured with DHT or E2. The expression of *Mib1* was induced only in MFs, whereas the expressions of *Ar* and *Esr2* were induced in both MCs and MFs (Fig 26a). Chromatin immunoprecipitation (ChIP) assays revealed that the AR-binding region of the *Mib1* promoter was unmethylated on histone H3 lysine 9 (H3K9) and H3K27 in MFs, whereas highly methylated in SCs. Consistently, AR and RNA polymerase II were recruited to the AR-binding region in MFs but not in SCs by DHT treatment (Fig. 26c). Together, these results show that AR and ERβ signaling can induce Mib1 expression in MFs, but not in SCs, possibly due to the different histone modifications within the *Mib1* promoter.

To test whether AR and ERβ signaling regulate SC populations, I examined $Ar^{\Delta MF}Esr2^{-/-}$ mice in which the serum levels of testosterone

and estradiol were comparable to control (Fig. 29a, b). The expression of Mib1 decreased in 4-week-old $Ar^{\Delta MF}$ and $Ar^{\Delta MF}Esr2^{-/-}$ MFs compared to control and $Esr2^{-/-}$ MFs (Fig. 29c). Consistently, the expression levels of *Ar*, *Esr2* in MFs and Notch target genes in MCs also decreased in $Ar^{\Delta MF}Esr2^{-/-}$ mice (Fig. 28). Indeed, the number of quiescent SCs markedly decreased in 4-week-old $Ar^{\Delta MF}$ and $Ar^{\Delta MF}Esr2^{-/-}$ TA muscles, compared to those of other groups (Fig. 30a, b). Residual quiescent SCs in $Ar^{\Delta MF}Esr2^{-/-}$ mice might be due to the incomplete recombination of *Ar* floxed gene (Bao et al., 2013; Maatta et al., 2013) or *Esr2* transcription variants (Dupont et al., 2000) resulting in Mib1 induction (Fig. 28e). While Mib1 expression and quiescent SC numbers in 4-week-old $Ar^{\Delta MF}$ mice decreased compared to those of controls, a substantial number of quiescent SCs in 8-week-old $Ar^{\Delta MF}$ muscles exists (Fig. 28c and 29c). This considerable number of SCs in $Ar^{\Delta MF}$

mice may result from the delayed increase of E2 after puberty (Fig. 31c). Flow cytometry analysis also showed that Vcam-1^{+}Sca-1^{-} populations significantly decreased in Ar$^{\Delta MF}$Esr2$^{-/-}$ muscles (Fig. 30c). These results show that AR and ERβ signaling induce Mib1 expression in MFs to regulate the conversion of juvenile SCs into adult quiescent SCs.

Sex hormones establish adult SC populations

To investigate whether sex hormones can affect the establishment of quiescent SC populations, the release of sex hormones was surgically [orchiectomy (Orx) at 2 weeks of age] and pharmacologically [a Nal-Lys gonadotropin releasing-hormone antagonist (Antide)](Edelstein et al., 1990) inhibited before puberty (Fig. 31a). The levels of testosterone and E2, and the expression levels of *Mib1*, and Notch target genes considerably decreased in Orx and Antide-treated mice compared to

controls (Fig. 31b-d). Consistently, the majority of $Pax7^+$ cells were still proliferating in 4-week-old Orx and Antide-treated TA muscles (Fig. 32), and the number of quiescent $Pax7^+$ SCs significantly decreased in 8-week-old TA muscles (Fig. 32c). To confirm these observations, I further used Gonadotrophin-releasing hormone-deficient hypogonadal (*Gnrh1*$^{hpg/hpg}$) mice (Fig. 33), in which the release of sex hormones was reduced (Cattanach et al., 1977) (Fig. 34a, b). Notably, the number of quiescent $Pax7^+$ cells markedly decreased in *Gnrh1*$^{hpg/hpg}$ mice, corresponding to the levels of sex hormones and the expression levels of sex hormone receptors, *Mib1*, and Notch target genes (Fig. 35a-c). Consistently, flow cytometric analysis revealed that $Vcam1^+Sca\text{-}1^-$ cells and $Pax7^+$ SCs decreased in Orx, Antide-treated and *Gnrh*$^{hpg/hpg}$ mice compared to controls (Fig. 35d, e), showing that sex hormones of the hypothalamic-pituitary-gonadal axis at puberty are required for the

establishment of quiescent adult SC populations.

Sex hormones re-establish adult SC populations upon injury

To investigate whether the sex hormones-Notch signaling axis is also implicated in the maintenance of quiescent SC populations in adult, I castrated 12-week-old mice or treated them with Antide. The inhibitory effects of sex hormones were confirmed by gross morphology of LA muscles (Fig. 36a, b). However, the cross-sectional area (CSA) of TA muscle myofibers was comparable between groups (not shown). Also the number of $Pax7^{+}$ cells were comparable between groups even 8 weeks after Orx or Antide treatment (Fig. 36c, d), suggesting that the sex hormone-Notch signaling axis is dispensable for the maintenance of adult SCs. To examine whether sex hormones are required for the re-establishment of quiescent SC populations, I injured TA muscles of Orx

or Antide-treated mice with $BaCl_2$. Although the CSA of the myofiber were comparable between groups after regeneration (Fig. 37a), $Pax7^+EdU^+$ cells increased in Orx or Antide-treated mice compared to controls after 14 days of muscle injury whereas $Pax7^+EdU^-$ cells decreased (Fig. 37b, c), suggesting that repopulating SCs in the hormone-reduced mice still remain in activated state. Indeed, at day 21 following muscle injury, in which self-renewal and homeostasis are being re-established(Kuang et al., 2007; Mourikis et al., 2012b; Shea et al., 2010), the populations of SCs were significantly reduced in Orx or Antide-treated mice (Fig. 37d, e).

In order to confirm whether DHT can rescue adult quiescent SC population after injury, 12-week-old mice were castrated and implanted with DHT. TA muscles of these mice were injured with $BaCl_2$ 3 days

after Orx, and then analyzed 30 days after muscle injury (Fig. 38a and b). In accordance with our data showing decreased number of SCs after muscle regeneration in hormone-reduced mice, the administration of DHT to Orx mice significantly restored the SC population after muscle regeneration (Figure 38c and d). The mean CSA of regenerated myofibers in the Orx mice treated with DHT was increased compared to those in Orx mice (P=0.0447, Figure 38e), which might be due to the anabolic effect of DHT on muscle growth (Yoo and Ko, 2012). Collectively, these results show that the sex hormone-Mib1-Notch signaling axis is required for the re-establishment of quiescent adult SC populations.

Figure 5. Conversion of cycling satellite cells (SCs) into quiescent SCs by dihydrotestosterone (DHT).

(a,b) Ten-day-old mice were subcutaneously (s.c.) injected with corn oil (Veh) or dihydrotestosterone (DHT). **(a)** Representative immunohistochemical (IHC) staining for Pax7 and Ki67 in *tibialis anterior* (TA) muscles. Arrows and arrowheads indicate $Pax7^{+}Ki67^{+}$ and $Pax7^{+}Ki67^{-}$ cells, respectively (n=5 animals for each group; scale bar, 20 μm). **(b)** mRNA expressions of SCs isolated from hindlimb muscles 3 days after treatment (n=3 biologically independent experiments from 3 animals for each group; Data are mean ± SD; two sample *t*-test; $*P < 0.05$). **(c)** Quantification of $Pax7^{+}Ki67^{+}$ and $Pax7^{+}Ki67^{-}$ cells per 100 myofibers (MFs) (n=3 biologically independent experiments from 5 biologically animals for each group; Data are mean ± SD; Bootstrap *t*-test; $*P < 0.05$). **(d,e)** Representative immunohistochemical (IHC) staining for Pax7, p57 (d) MyoD and Ki67 (e) in *tibialis anterior* (TA) muscles (n=5 animals for each group; scale bar, 25 μm).

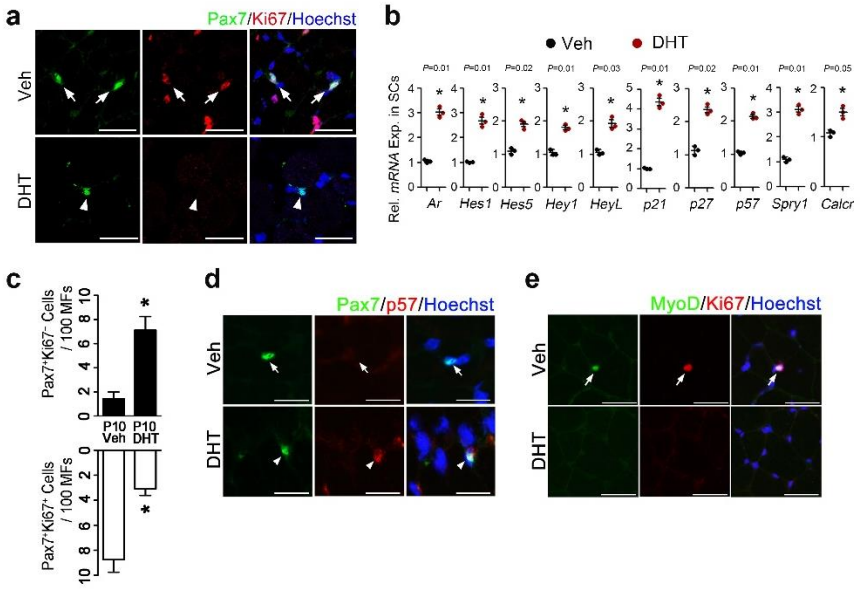
a
Pax7/Ki67/Hoechst
Veh
DHT
b
Veh
DHT
Rel. mRNA Exp. in SCs
P=0.01
P=0.01
P=0.02
P=0.01
P=0.03
P=0.01
P=0.02
P=0.01
P=0.01
P=0.05
Ar
Hes1
Hes5
Hey1
HeyL
p21
p27
p57
Spry1
Calcr
c
Pax7+Ki67- Cells / 100 MFs
P10 Veh
P10 DHT
Pax7+Ki67+ Cells / 100 MFs
d
Pax7/p57/Hoechst
Veh
DHT
e
MyoD/Ki67/Hoechst
Veh
DHT

\

Figure 6. Gene expression profiling of skeletal muscles after dihydrotestosterone (DHT) treatment.

Microarray analysis of Veh or DHT-injected 10-day-old mice s.c. injected with Veh or DHT [GSE64454]. TA muscles were isolated 24 h after the injection. The significantly upregulated genes identified from an independent dataset are depicted as a Venn diagram **(a)**. Selected microarray datasets: 1) Adult SCs in uninjured muscle compared to SCs in injured muscle [GSE47177(Liu et al., 2013)], 2) quiescent SCs compared to activated SCs in culture conditions [GSE3483(Fukada et al., 2007)], and 3) TA muscles of 10-day-old male mice injected with DHT compared to Veh. Venn diagrams display the number of common genes obtained from the gene expression dataset. Integrative analysis **(b)**. In total 1,031 genes were found to be significantly increased (>2-fold) or decreased (<-2-fold) in Veh and DHT-treated mice. These datasets were used as input for pathway analysis with the Ingenuity pathway analysis (IPA) software (Ingenuity® Systems, http://www.ingenuity.com, Redwood City, CA, USA). The graph with the most significant *p*-values, and the highest-scoring functional pathways are shown. **(c)** The pathway analysis of Notch signaling and cell cycle-related genes that are expressed at a substantially higher or lower level in DHT-injected TA muscles than in Veh-injected TA muscles. The pathway analysis via IPA software is depicted as containing the majority of Notch signaling-regulated genes. The analysis was performed with the Ingenuity software package. Red and green circles represent upregulated and downregulated genes, respectively.

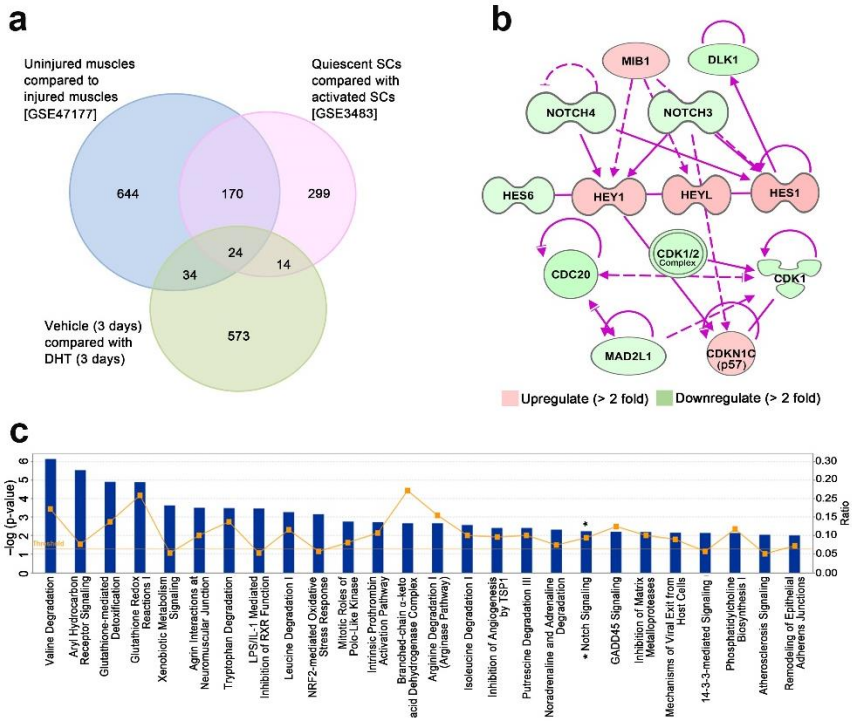
a
Uninjured muscles compared to injured muscles [GSE47177]
Quiescent SCs compared with activated SCs [GSE3483]
Vehicle (3 days) compared with DHT (3 days)
644
170
299
24
34
14
573
b
MIB1
DLK1
NOTCH4
NOTCH3
HES6
HEY1
HEYL
HES1
CDK1/2 Complex
CDC20
CDK1
MAD2L1
CDKN1C (p57)
Upregulate (> 2 fold)
Downregulate (> 2 fold)
c
−log (p-value)
Ratio
Valine Degradation
Aryl Hydrocarbon Receptor Signaling
Glutathione-mediated Detoxification
Glutathione Redox Reactions I
Xenobiotic Metabolism Signaling
Agrin Interactions at Neuromuscular Junction
Tryptophan Degradation
LPS/IL-1 Mediated Inhibition of RXR Function
Leucine Degradation I
NRF2-mediated Oxidative Stress Response
Mitotic Roles of Polo-Like Kinase
Intrinsic Prothrombin Activation Pathway
Branched-chain α-keto acid Dehydrogenase Complex
Arginine Degradation I (Arginase Pathway)
Isoleucine Degradation I
Inhibition of Angiogenesis by TSP1
Putrescine Degradation III
Noradrenaline and Adrenaline Degradation
Notch Signaling
GADD45 Signaling
Inhibition of Matrix Metalloproteases
Mechanisms of Viral Exit from Host Cells
14-3-3-mediated Signaling
Phosphatidylcholine Biosynthesis I
Atherosclerosis Signaling
Remodeling of Epithelial Adherens Junctions

Figure 7. Notch1 activation in cycling satellite cells (SCs) at puberty

(a) Relative expression levels of Notch target genes in myogenic cells (MCs) at the indicated ages (n=3 representative lysates for each condition; Data are mean ± SD; Two-sample *t*-test; $*P < 0.05$). **(b)** IHC staining of Pax7 and Nicd in TA muscles at the indicated ages. **(c)** Quantification of Pax7 and Nicd in TA muscles as in **b** Arrows and arrowheads indicate $Nicd^{-}Pax7^{+}$ and $Nicd^{+}Pax7^{+}$ cells, respectively (n=3 animals for each group; Data are mean ± SD; scale bar, 25μm).

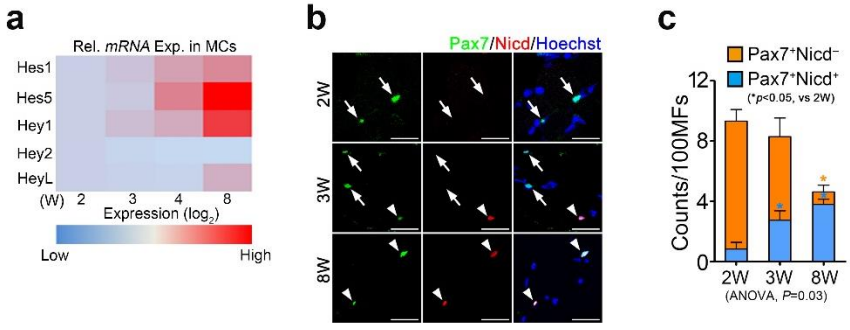
a
Rel. mRNA Exp. in MCs
Hes1
Hes5
Hey1
Hey2
HeyL
(W) 2 3 4 8
Expression (log2)
Low
High
b
Pax7/Nicd/Hoechst
2W
3W
8W
c
Pax7+Nicd−
Pax7+Nicd+
(*p<0.05, vs 2W)
Counts/100MFs
12
8
4
0
2W 3W 8W
(ANOVA, P=0.03)

Figure 8. Conversion of cycling juvenile SCs into quiescent SCs by Notch signaling

(a) Representative IHC staining for Pax7, BrdU, and Nicd in 2- and 3-week-old TA muscles. Arrows and arrowheads indicate $Pax7^{+}BrdU^{+}Nicd^{-}$ and $Pax7^{+}BrdU^{-}Nicd^{+}$ cells, respectively (n=5 animals for each group; scale bar, 10 μm). **(b)** Quantification of Pax7, BrdU and Nicd in TA muscles as in **a** (n=3 biologically independent experiments from 3 animals for each group; Data are mean ± SD; Bootstrap *t*-test; $*P < 0.05$)

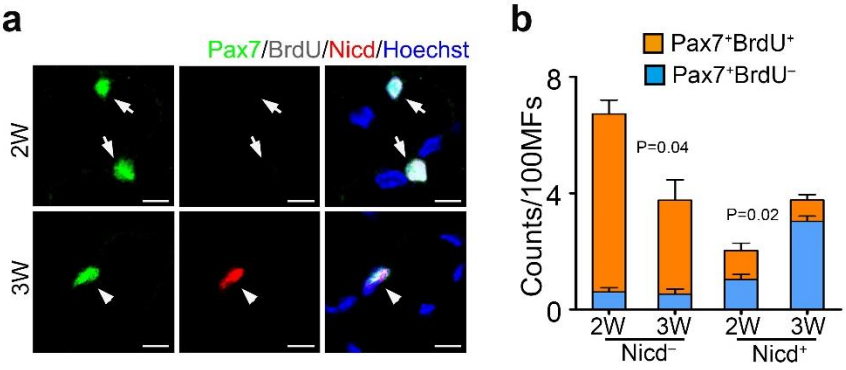
a
Pax7/BrdU/Nicd/Hoechst
2W
3W
b
Pax7⁺BrdU⁺
Pax7⁺BrdU⁻
Counts/100MFs
8
4
0
P=0.04
P=0.02
2W
3W
2W
3W
Nicd⁻
Nicd⁺

Figure 9. Requirement of Notch signaling for conversion of activating juvenile SCs to quiescent SCs

(a,b) Seven-day-old $N1^{WT}$ and $N1^{\Delta SC}$ mice were injected with tamoxifen for 3 days and analyzed at 4-week-old. **(a)** Representative IHC staining for Pax7 and Ki67 in TA muscles. Arrows and arrowheads indicate $Pax7^{+}Ki67^{+}$ and $Pax7^{+}Ki67^{-}$ cells, respectively (n=5 animals for each group; scale bar, 20 μm). **(b)** Quantification of Pax7 and Ki67 in TA muscles as in **a** (n=3 biologically independent experiments from 3 animals for each group; Data are mean ± SD; Bootstrap t-test; $*P < 0.05$).

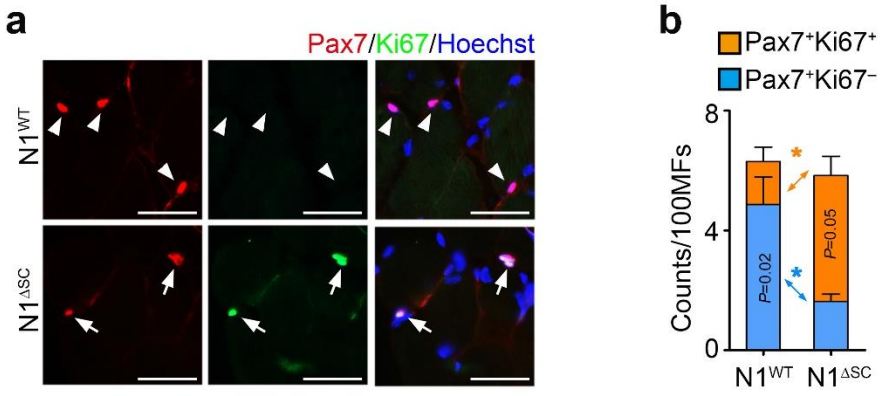
a
Pax7/Ki67/Hoechst
N1WT
N1ΔSC
b
Pax7+Ki67+
Pax7+Ki67−
Counts/100MFs
8
4
0
P=0.02
P=0.05
N1WT
N1ΔSC

Figure 10. Gene expression profiling of *Notch1* lacking SCs.

Expression of QSC related genes (*p21*, *p27*, *p57*, *Spry1* and *Calcr*) and muscle regulating factors (*Pax7*, *MyoD* and *MyoG*) in purified SCs from TA muscles (n=3 biologically independent experiments; Data are mean ± SD; two sample *t*-test; $*P < 0.05$).

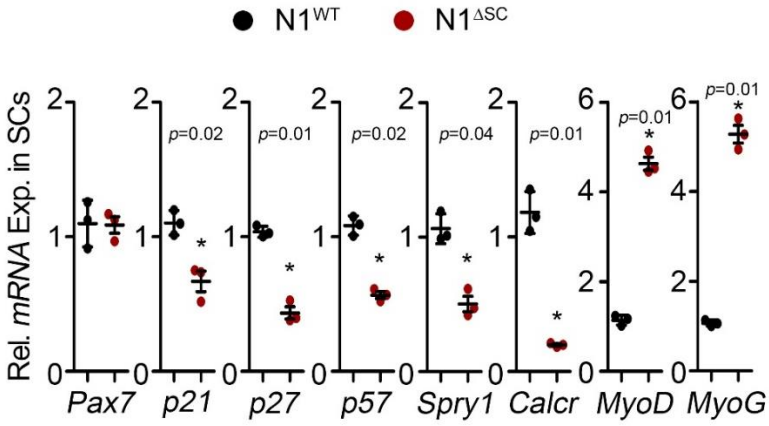
N1WT
N1ΔSC
Rel. mRNA Exp. in SCs
p=0.02
p=0.01
p=0.02
p=0.04
p=0.01
p=0.01
p=0.01
Pax7
p21
p27
p57
Spry1
Calcr
MyoD
MyoG

Figure 11. Specific requirement of Notch1 signaling for establishment of quiescent SCs

Relative muscle mass normalized to body weight **(a)**, mRNA expression in MCs **(b)**, IHC staining of Pax7 **(c)** (n=3 biologically independent experiments from 3 animals for each group; Data are mean ± SD; Two-sample *t*-test; **P* < 0.05; scale bar, 50μm). Relative muscle masses to body weights were comparable.

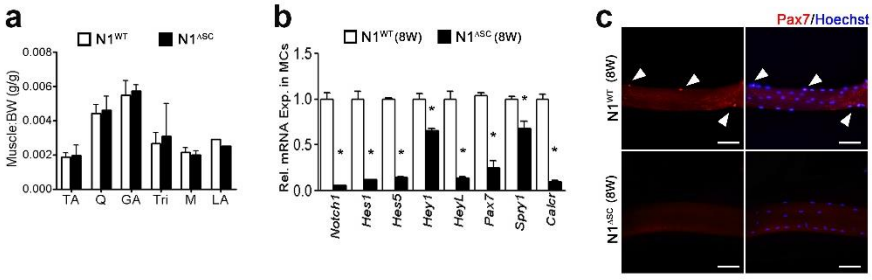
a
N1WT
N1ΔSC
Muscle BW (g/g)
0.008
0.006
0.004
0.002
0.000
TA
Q
GA
Tri
M
LA
b
N1WT (8W)
N1ΔSC (8W)
Rel. mRNA Exp. in MCs
1.5
1.0
0.5
0.0
Notch1
Hes1
Hes5
Hey1
HeyL
Pax7
Spry1
Calcr
c
Pax7/Hoechst
N1WT (8W)
N1ΔSC (8W)

Figure 12. Notch activation converts cycling SCs to quiescent SCs.

Seven-day-old $N1^{WT}$ and $N1^{OE/SC}$ mice were intraperitoneally (i.p.) injected daily with tamoxifen for 3 days. Nicd and nuclear GFP proteins are expressed in the $Pax7^+$ cells of $N1^{OE/SC}$ mice. **(a)** Representative IHC staining for Pax7, GFP, and Ki67 from 10-day-old $N1^{WT}$ and $N1^{OE/SC}$ TA muscles. Arrows and arrowheads indicate $Pax7^+GFP^-Ki67^+$ and $Pax7^+GFP^+Ki67^-$ cells, respectively (n=3 animals for each group; scale bar, 25 μm). **(b)** Quantification of Pax7, GFP, and Ki67 as in **a** (n=117 SCs for $N1^{WT}$; n=194 SCs for $N1^{OE/SC}$; n=3 biologically independent experiments; Data are mean ± SD).

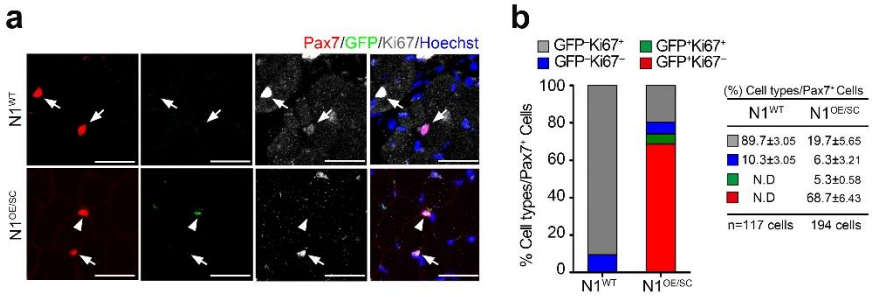
a
Pax7/GFP/Ki67/Hoechst
N1WT
N1OE/SC
b
GFP-Ki67+
GFP+Ki67+
GFP-Ki67-
GFP+Ki67-
% Cell types/Pax7+ Cells
100
80
60
40
20
0
N1WT
N1OE/SC
(%) Cell types/Pax7+ Cells
N1WT
N1OE/SC
89.7±3.05
19.7±5.65
10.3±3.05
6.3±3.21
N.D
5.3±0.58
N.D
68.7±6.43
n=117 cells
194 cells

Figure 13. Notch activation converts cycling SCs to quiescent SCs through exit of cell cycle.

Seven-day-old $N1^{WT}$ and $N1^{OE/SC}$ mice were intraperitoneally (i.p.) injected daily with tamoxifen for 3 days. IHC staining (**a**; scale bar, 25 μm) and quantification of Pax7, GFP, and p57 (**b**) from 10-day-old $N1^{WT}$ and $N1^{OE/SC}$ TA muscles. Nicd and nuclear GFP proteins are expressed in the $Pax7^{+}$ cells of $N1^{OE/SC}$ mice. Arrows and arrowheads indicate $Pax7^{+}GFP^{-}p57^{-}$ and $Pax7^{+}GFP^{+}p57^{+}$ cells, respectively (n=3 biologically independent experiments from 3 animals for each group; scale bar, 25μm).

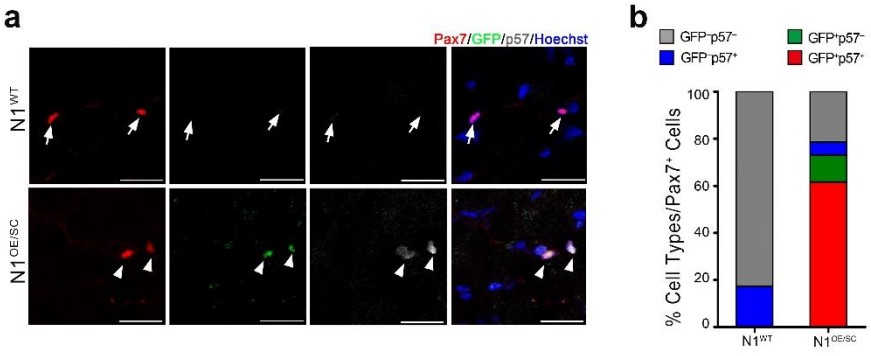
a
Pax7/GFP/p57/Hoechst
N1WT
N1OE/SC
b
GFP-p57-
GFP+p57-
GFP-p57+
GFP+p57+
% Cell Types/Pax7+ Cells
100
80
60
40
20
0
N1WT
N1OE/SC

Figure 14. Expression of Notch signaling components in myogenic cells (MCs) and myofibers (MFs)

Immunoblotting of myogenic cells (MCs) and MFs from wild-type hindlimb muscles at 4-week-old **(a)** or indicated ages **(b, c)**.

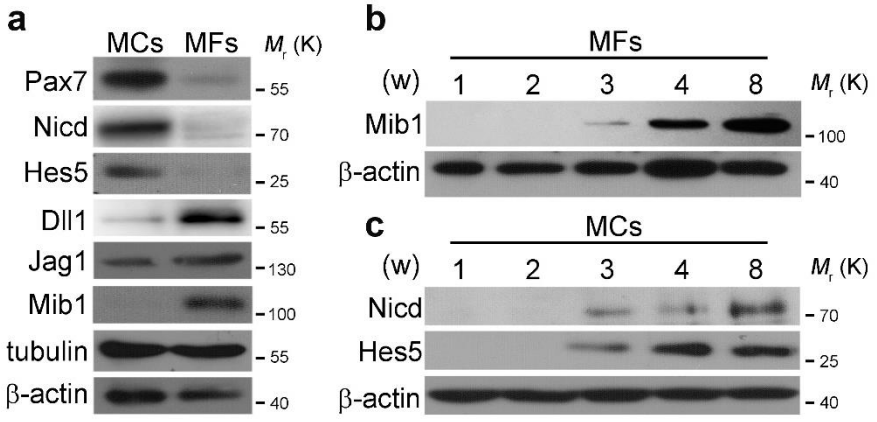
a
MCs
MFs
M_r (K)
Pax7
Nicd
Hes5
Dll1
Jag1
Mib1
tubulin
β-actin
55
70
25
55
130
100
55
40
b
MFs
(w)
1
2
3
4
8
M_r (K)
Mib1
β-actin
100
40
c
MCs
(w)
1
2
3
4
8
M_r (K)
Nicd
Hes5
β-actin
70
25
40

Figure 15. Analysis of the hindlimb muscles lacking *Mib1* in myofibers.

The expression of *Mib1* (**a**; n=3 biologically independent experiments from n=5 animals for each group; Data are mean ± SD; Two-sample *t*-test; $*P < 0.05$), IHC staining for Mib1 (**b**; n= 5 animals for each group; scale bar, 25μm), and myonuclei number (**c**; n=3 biologically independent experiments from 5 animals for each group; Data are mean ± SD; Poisson's general linear model regression; N.S. not significant) in MFs from 8-week-old $Mib1^{WT}$ and $Mib1^{\Delta MF}$ *extensor digitorum longus* (EDL) muscles. Myonuclei numbers in $Mib1^{WT}$ and $Mib1^{\Delta MF}$ MFs were comparable. **(d)** Morphometric quantification of cross-sectional area validated in Laminin-stained TA muscles, which is comparable in $Mib1^{WT}$ and $Mib1^{\Delta MF}$ mice (n=5 animals for each group; Data are mean ± SD; χ^2 test).

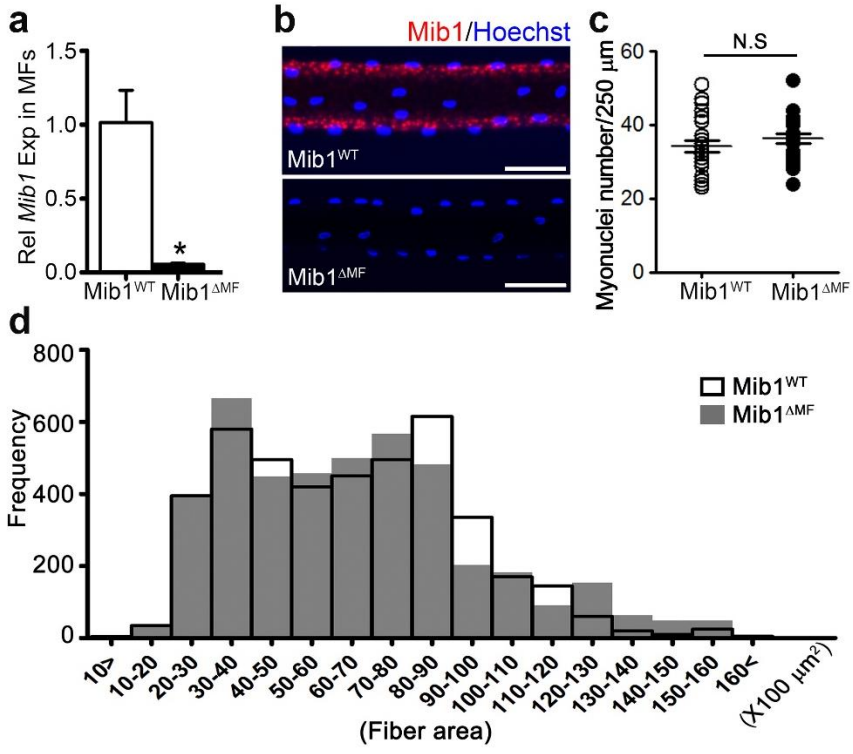
a
Rel Mib1 Exp in MFs
1.5
1.0
0.5
0.0
*
Mib1WT
Mib1ΔMF
b
Mib1/Hoechst
Mib1WT
Mib1ΔMF
c
N.S
Myonuclei number/250 μm
60
40
20
0
Mib1WT
Mib1ΔMF
d
Frequency
800
600
400
200
0
Mib1WT
Mib1ΔMF
10>
10-20
20-30
30-40
40-50
50-60
60-70
70-80
80-90
90-100
100-110
110-120
120-130
130-140
140-150
150-160
160<
(X100 μm²)
(Fiber area)

Figure 16. Defective Notch activation of SCs by *Mib1*-null MF

Immunoblotting of SCs and MFs from $Mib1^{WT}$ and $Mib1^{\Delta MF}$ hindlimb muscles at 4-week-old five representative lysates for each condition. **(b)** Representative IHC staining for Pax7 and Nicd in TA muscles from 4-week-old $Mib1^{WT}$ and $Mib1^{\Delta MF}$ mice. Arrows and arrowheads indicate $Pax7^{+}Nicd^{-}$ and $Pax7^{+}Nicd^{+}$ cells, respectively (n=3 animals for each group; scale bar, 20 μm). **(c)** Quantification of Pax7, Nicd as in **b** (n=3 biologically independent experiments from 3 animals for each group; Data are mean ± SD; Bootstrap *t*-test; $^{**}P < 0.01$).

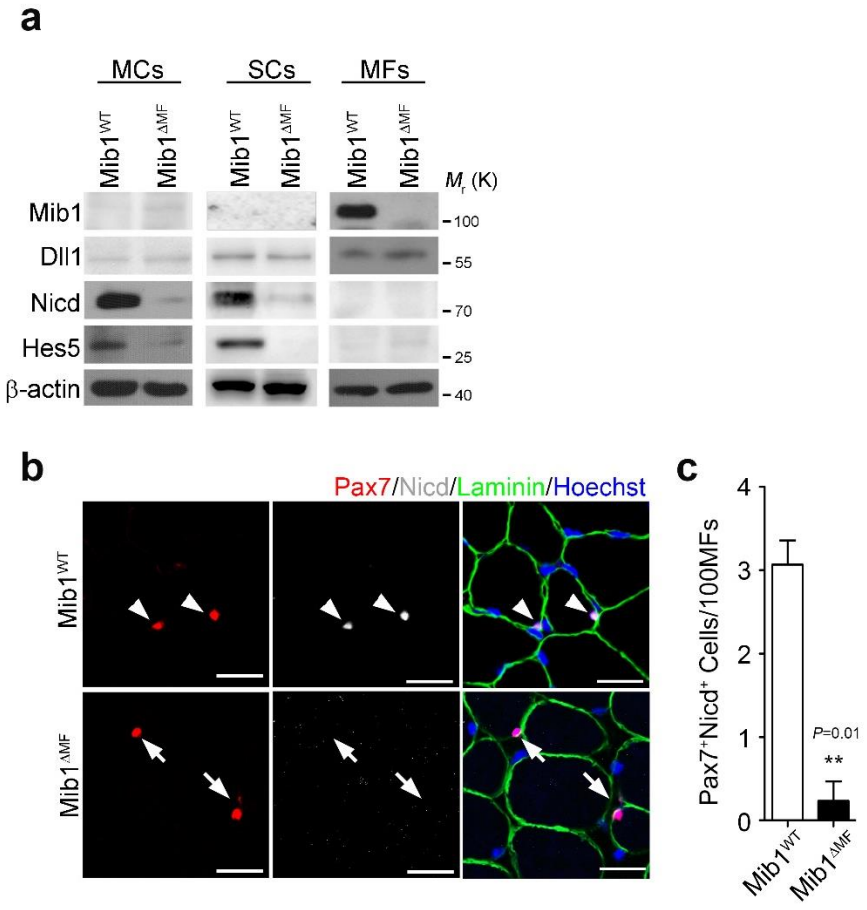
a
MCs
SCs
MFs
Mib1WT
Mib1ΔMF
Mr (K)
Mib1
Dll1
Nicd
Hes5
β-actin
100
55
70
25
40
b
Pax7/Nicd/Laminin/Hoechst
Mib1WT
Mib1ΔMF
c
Pax7+Nicd+ Cells/100MFs
P=0.01
**
Mib1WT
Mib1ΔMF

Figure 17. Failure induction of QSC related genes in SCs of Mib1$^{\Delta MF}$ mice

Expressions of QSC related genes (*p21*, *p27* and *Spry1*) in purified MCs from TA muscles at indicated age (n=3 biologically independent experiments; Data are mean ± SD; two sample *t*-test; *$P < 0.05$).

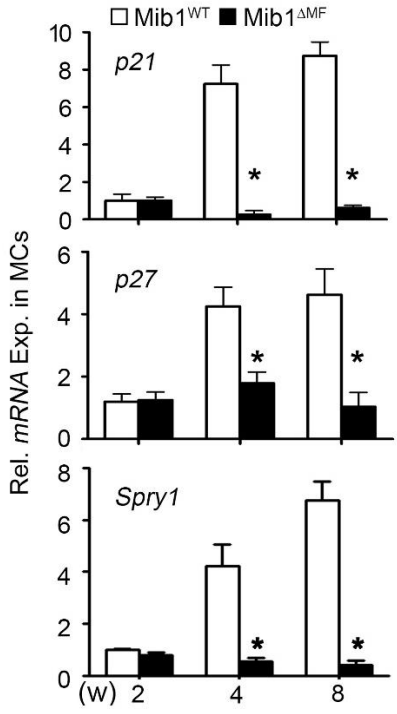
Mib1WT
Mib1ΔMF
p21
p27
Spry1
Rel. mRNA Exp. in MCs
(w) 2
4
8
*

Figure 18. Gene expression profiling in SCs of Mib1^{WT} and Mib1$^{\Delta MF}$ mice

mRNA expressions of *Pax7*, Notch target genes, differentiation markers, and stem cell markers in SCs purified from 4-week-old Mib1^{WT} and Mib1$^{\Delta MF}$ mice (n=3 biologically independent experiments from 5 animals for each group; Data are mean ± SD; Two-sample *t*-test; *$P < 0.05$).

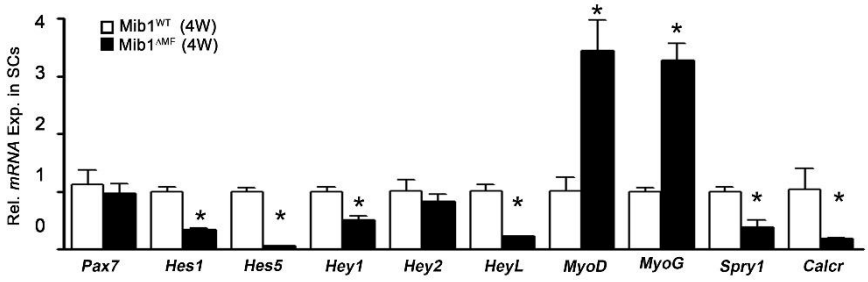
Mib1WT (4W)
Mib1ΔMF (4W)
Rel. mRNA Exp. in SCs
4
3
2
1
0
*
Pax7
Hes1
Hes5
Hey1
Hey2
HeyL
MyoD
MyoG
Spry1
Calcr

Figure 19. Persistent cell cycling and myogenic activation in SCs Mib1$^{\Delta MF}$ mice

(a) IHC staining for MyoD and Ki67 in TA muscles from Mib1^{WT} and Mib1$^{\Delta MF}$ mice at the indicated ages. Arrows indicate MyoD^{+}Ki67^{+} cells (n=5 animals for each group; scale bar, 25μm). **(b)** Quantification of MyoD^{+} cells per 100 MFs in TA muscles of Mib1^{WT} and Mib1$^{\Delta MF}$ mice at indicated ages (n=5 animals for each group; Data are mean ± SD; Two-sample *t*-test; * P <0.05).

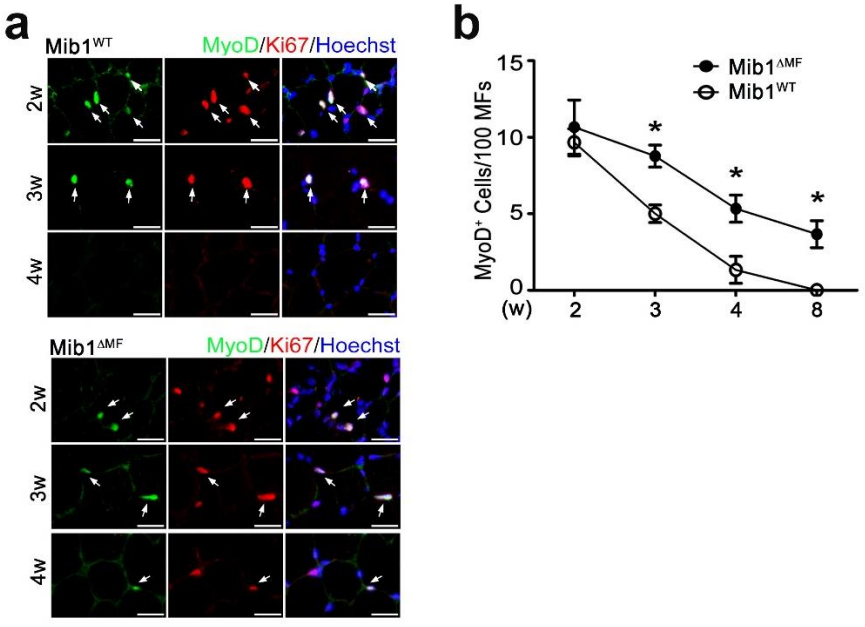
a
Mib1WT
MyoD/Ki67/Hoechst
2w
3w
4w
Mib1ΔMF
MyoD/Ki67/Hoechst
2w
3w
4w
b
Mib1ΔMF
Mib1WT
MyoD+ Cells/100 MFs
15
10
5
0
(w)
2
3
4
8
*
*
*

Figure 20. MF-specific *Mib1* ablation affects differentiation of SCs

(a) Representative IHC staining for Pax7 and MyoG in $Mib1^{WT}$ and $Mib1^{\Delta MF}$ TA muscles. Arrows and arrowheads indicate $Pax7^{+}MyoG^{-}$ and $Pax7^{+}MyoG^{+}$ cells, respectively (n=3 animals for each group; scale bar, 20 μm). **(b)** Quantification of Pax7 and MyoG as in **g** (n=3 biologically independent experiments from 3 animals for each group; Data are mean ± SD; Bootstrap *t* test; $*P < 0.05$). **(c)** Pax7 and MyoG in TA muscles from 4- and 12-week-old $Mib1^{WT}$ mice. The $Pax7^{+}/MyoG^{+}$ cells were observed only in 4-week-old. **(d)** Immunoblotting of Myogenin in SCs isolated from hindlimb muscles of 4-week-old $Mib1^{WT}$ and $Mib1^{\Delta MF}$ mice. Numbers represent the relative signal intensity of the designated antibody measured by densitometry (n=5 representative lysates for each condition).

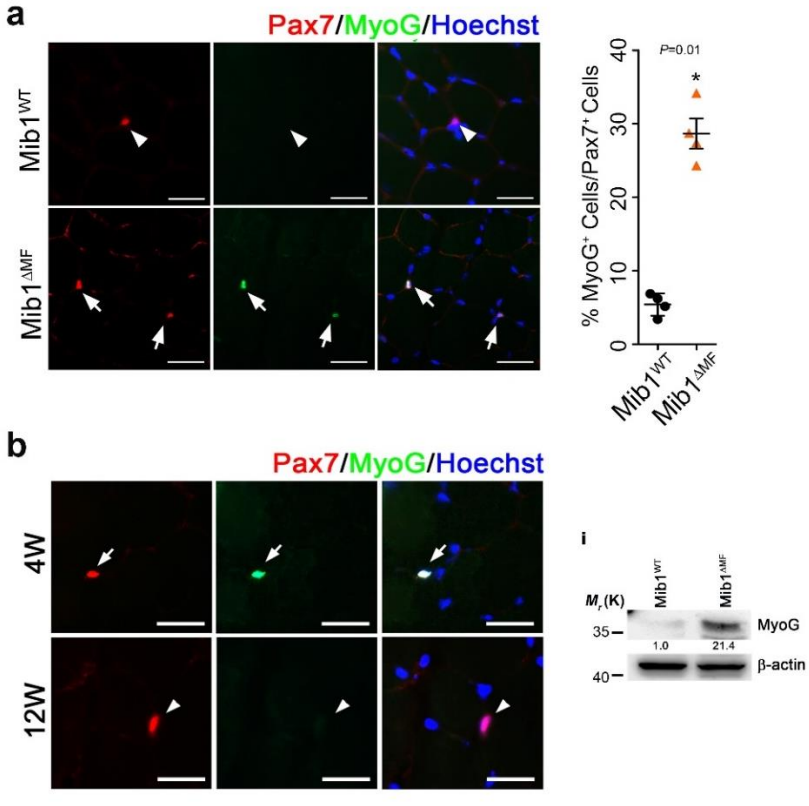
a
Pax7/MyoG/Hoechst
Mib1WT
Mib1ΔMF
P=0.01
*
% MyoG+ Cells/Pax7+ Cells
0
10
20
30
40
Mib1WT
Mib1ΔMF
b
Pax7/MyoG/Hoechst
4W
12W
i
Mr(K)
Mib1WT
Mib1ΔMF
35
40
MyoG
β-actin
1.0
21.4

Figure 21. MF-specific *Mib1* ablation affects precocious depletion of SCs in hindlimb muscles and defective muscle regeneration.

(a) IHC staining for Pax7 and Ki67 in TA muscles from $Mib1^{WT}$ and $Mib1^{\Delta MF}$ mice at the indicated ages (n=5 animals for each group; scale bar, 50 μm). Arrows and arrowheads indicate $Ki67^{+}Pax7^{+}$ and $Ki67^{-}Pax7^{+}$ cells, respectively. **(b)** Quantification of $Pax7^{+}Ki67^{+}$ and $Pax7^{+}Ki67^{-}$ cells in TA muscles of indicated genotypes and ages (n=3 biologically independent experiments from 5 animals for each group; Data are mean ± SD; Bootstrap *t*-test; $*P < 0.05$, $**P < 0.01$).

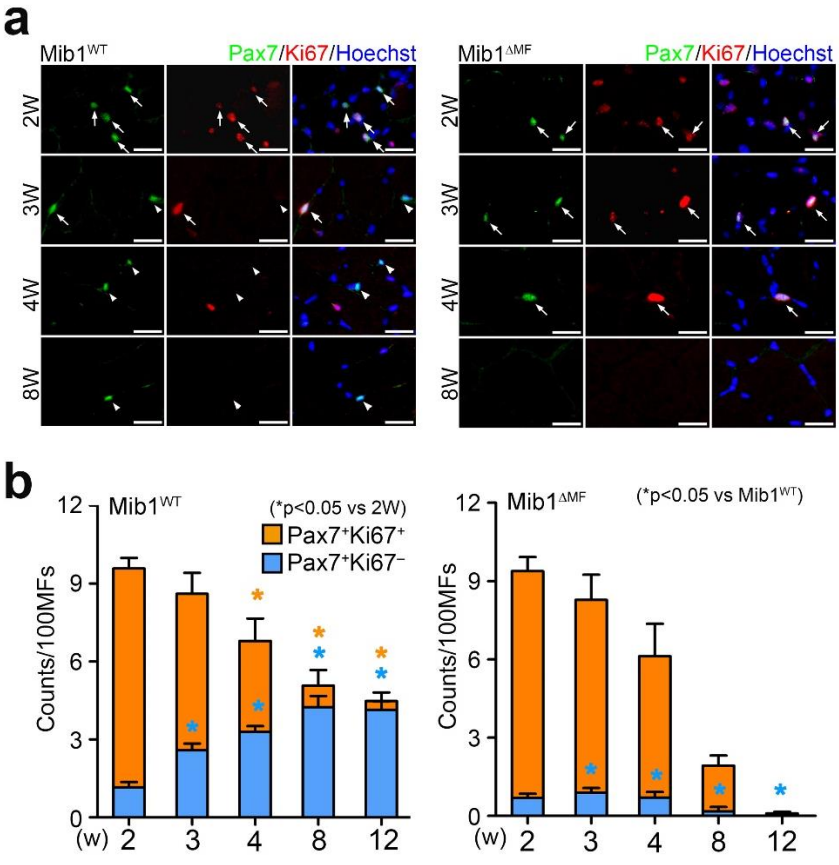
a
Mib1WT
Pax7/Ki67/Hoechst
Mib1ΔMF
Pax7/Ki67/Hoechst
2W
3W
4W
8W
b
Mib1WT
(*p<0.05 vs 2W)
Pax7+Ki67+
Pax7+Ki67−
Counts/100MFs
(w) 2 3 4 8 12
Mib1ΔMF
(*p<0.05 vs Mib1WT)

Figure 22. Analysis of adult muscle stem cell population in Mib1$^{\Delta MF}$ and N1$^{\Delta SC}$ mice.

Flow cytometric analysis of SC populations ($Lin^{-}Sca1^{-}Vcam1^{+}$) in 8-week-old $Cont^{WT}$ ($Mib1^{WT}$ and $N1^{WT}$), $Mib1^{\Delta MF}$, and $N1^{\Delta SC}$ mice (n=5 animals for each group; Data are mean ± SD; Tukey's pairwise comparison test; $^{**}P < 0.01$). Controls are designated as the WT of comparing mutant mice.

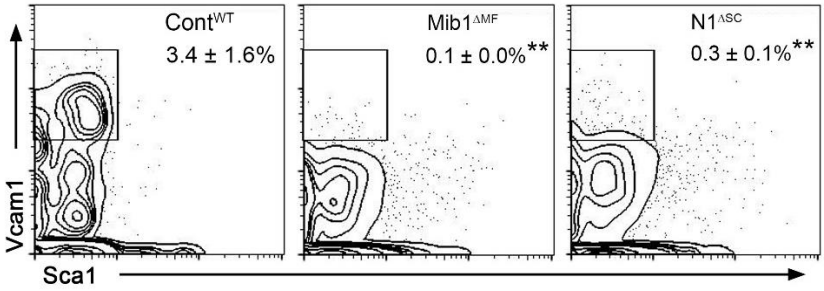
Cont^WT
3.4 ± 1.6%
Mib1^ΔMF
0.1 ± 0.0%**
N1^ΔSC
0.3 ± 0.1%**
Vcam1
Sca1

Figure 23. Defective regeneration in Mib1$^{\Delta MF}$ mice due to loss of SCs

(a) Optic (c; scale bar, 0.2 cm) and hematoxylin and eosin-stained (**b**; n=5 animals for each group; scale bar, 25 μm) images of $BaCl_2$-injured TA muscles in 8-week-old mice. (**c)** IHC stained images for Laminin in TA muscles 5 or 10 days after $BaCl_2$ injury (n=5 animals for each group; scale bar, 25 μm).

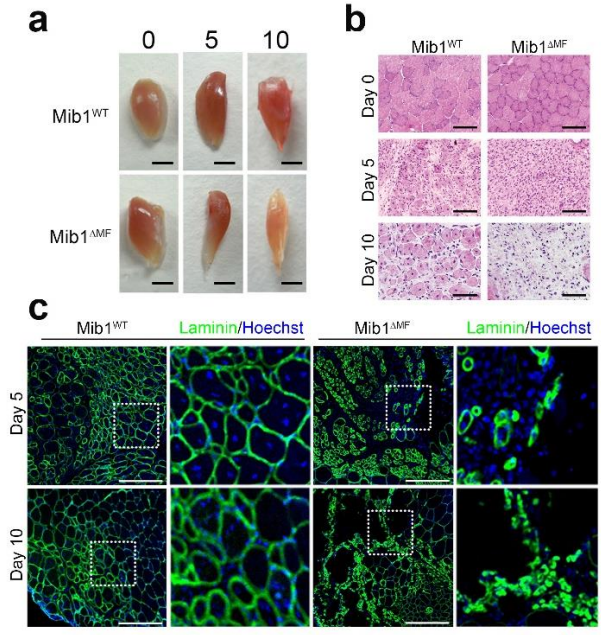
a
0
5
10
Mib1WT
Mib1ΔMF
b
Mib1WT
Mib1ΔMF
Day 0
Day 5
Day 10
c
Mib1WT
Laminin/Hoechst
Mib1ΔMF
Laminin/Hoechst
Day 5
Day 10

Figure 24. Sex hormones transcriptionally regulate *Mib1* expression

(a) A schematic diagram of the *Mib1* promoter region. Androgen response elements (AREs) and estrogen response elements (EREs) are indicated. The MT-ARE, MT-ERE, and double-mutant (dMT) constructs were generated with point mutations. The PCR primer sets used for chromatin immunoprecipitation (ChIP) assays are shown. C2C12 cells were transfected with wild-type and mutant plasmid constructs. Luciferase activity was measured 24h after ethanol (Veh), DHT, or E2 treatment (n=3 biologically independent cell culture per group; Data are mean ± SD; two sample *t*-test; $*P < 0.05$, $**P < 0.01$). **(b)** *Mib1* levels in MFs isolated from *extensor digitorum longus* (EDL) of 10-day-old mice. MFs were cultured with DHT and/or E2 in dosages shown in logarithmic scale for 12h (n=3, Data are mean ± SD).

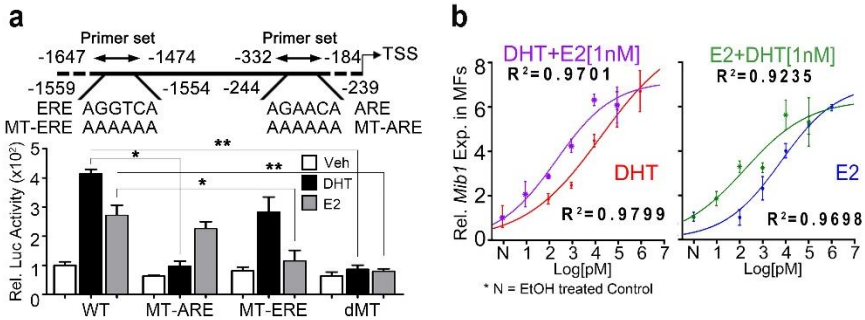
a
Primer set
Primer set
-1647
-1474
-332
-184
TSS
-1559
-1554
-244
-239
ERE AGGTCA
AGAACA ARE
MT-ERE AAAAAA
AAAAAA MT-ARE
Rel. Luc Activity (x10²)
Veh
DHT
E2
WT
MT-ARE
MT-ERE
dMT
b
DHT+E2[1nM]
R²=0.9701
DHT
R²=0.9799
E2+DHT[1nM]
R²=0.9235
E2
R²=0.9698
Rel. Mib1 Exp. in MFs
Log[pM]
Log[pM]
* N = EtOH treated Control

Figure 25. *Esr2*, not *Esr1* regulates *Mib1* expression in MFs

(a,b) Expression of *Mib1* in MFs from 10-day-old *MCK-Cre* (Ar^{WT}) or $Ar^{\Delta MF}$ mice in presence of E2 alone or E2 with inhibitors. MFs were isolated from hindlimb muscles and cultured with ethanol (Veh), E2, or E2 with 1,3-bis(4-hydroxyphenyl)-4-methyl-5-[4-(2-piperidinylethoxy)phenol]-1H-pyrazole-dihydrochloride (MPP, **a**) or 4-(2-phenyl-5,7-bis(trifluoromethyl)-pyrazolo[1,5-a]pyrimidin-3-yl)-phenol (PHTPP, **b**) for 24 h (n=3 biologically independent experiments from 200 myofibers for each group; Data are mean ± SD; two sample *t*-test; $*P < 0.05$, N.S. not significant). **(c)** *Mib1* levels in MFs from 4-week-old $Cont^{WT}$, $Esr2^{-/-}$, $Ar^{\Delta MF}$ and $Ar^{\Delta MF}Esr2^{-/-}$ EDL muscles 12h after culture with Veh, DHT or E2. Controls are designated as the WT of comparing mutant mice (n=3 biologically independent experiments from 5 animals for each group; Data are mean ± SD; two sample *t*-test; $*P < 0.05$).

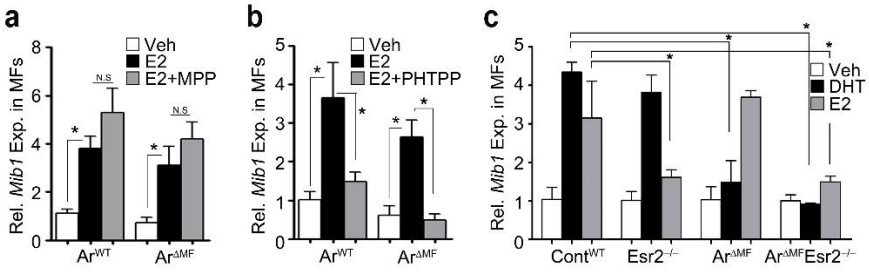
a
Rel. Mib1 Exp. in MFs
Veh
E2
E2+MPP
N.S
N.S
ArWT
ArΔMF
b
Rel. Mib1 Exp. in MFs
Veh
E2
E2+PHTPP
ArWT
ArΔMF
c
Rel. Mib1 Exp. in MFs
Veh
DHT
E2
ContWT
Esr2−/−
ArΔMF
ArΔMFEsr2−/−

Figure 26. Sex hormones induce *Mib1* in MFs but not SCs due to epigenetic status.

(a,b) *Mib1*, *Ar*, or *Estrogen receptor β* (*Esr2*) levels. MCs and MFs isolated from 10-day-old hindlimb muscles were treated with DHT or E2 in hormone-free media (n=3 biologically independent experiments from 200 myofibers for each group; Data are mean ± SD; two sample *t*-test; $*P < 0.05$). **(c)** ChIP assays on ARE-binding site of the *Mib1* promoter. Ten-day-old mice were s.c. injected with Veh or DHT. SCs and MFs were isolated from hindlimb muscles 24h after injection (n=3 biologically independent experiments).

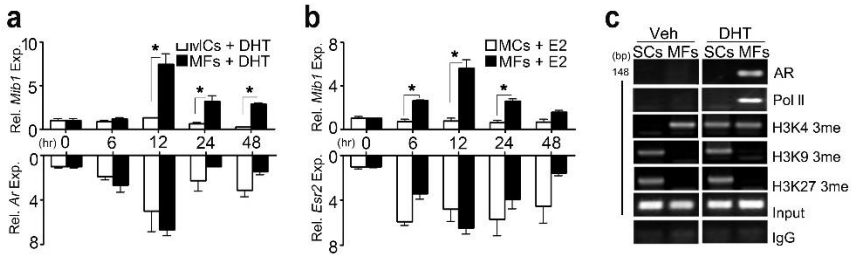
a
MCs + DHT
MFs + DHT
Rel. Mtb1 Exp.
Rel. Ar Exp.
(hr) 0 6 12 24 48
b
MCs + E2
MFs + E2
Rel. Mtb1 Exp.
Rel. Esr2 Exp.
(hr) 0 6 12 24 48
c
Veh
DHT
(bp)
148
SCs MFs SCs MFs
AR
Pol II
H3K4 3me
H3K9 3me
H3K27 3me
Input
IgG

Figure 27. E2 normally induces *Mib1* in MFs lacking *Ar*.

(a,b) The Cre-mediated recombination was confirmed by PCR in $Ar^{\Delta MF}$ mice at the indicated ages in the shown organs (a) and in myofiber but not in satellite cells (b) (n=3 for each group). **(c)** The gross morphology in *levator ani* (LA) muscles from 4-week-old $Ar^{\Delta MF}$ mice (n=3 animals for each group; scale bars, 0.5 cm). **(d,e)** IHC staining (d; n=3 animals for each group; scale bars, 20 μm), and quantification (e; n=3 biologically independent experiments from 3 animals for each group; Data are mean ± SD; Bootstrap *t*-test; $*P < 0.05$) for Pax7, Ki67, and Laminin in TA muscles from 10-day-old Ar^{WT} (upper) and $Ar^{\Delta MF}$ (bottom) mice injected with Veh or E2. TA muscles were isolated from hindlimb muscles 3 days after treatment. Arrows and arrowheads indicate $Ki67^{+}Pax7^{+}$ and $Ki67^{-}Pax7^{+}$ cells, respectively.

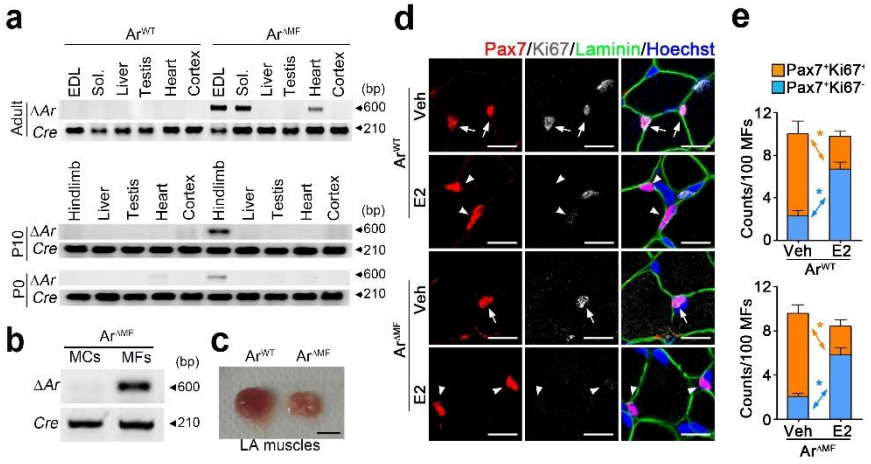
a
Ar^WT
Ar^ΔMF
EDL
Sol.
Liver
Testis
Heart
Cortex
(bp)
Adult
ΔAr
Cre
600
210
Hindlimb
P10
P0
b
Ar^ΔMF
MCs
MFs
c
LA muscles
d
Pax7/Ki67/Laminin/Hoechst
Veh
E2
e
Pax7+Ki67+
Pax7+Ki67-
Counts/100 MFs

Figure 28. Defective Notch activation of SCs by $Ar^{\Delta MF}Esr2^{-/-}$ dKO MF.

(a) Muscle mass (f; n=3 animals for each group; Data are mean ± SD; Two-sample *t*-test; **P* < 0.05), myonuclei numbers in MFs (**b**; n=3 biologically independent experiments from 3 animals for each group; Data are mean ± SD; Poisson's general linear model regression; N.S. not significant) of 12-week-old $Cont^{WT}$ and $Ar^{\Delta MF}Esr2^{-/-}$ mice. Muscle mass, myonuclei numbers were comparable. **(c)** Mib1 levels in 12-week-old EDL muscles from indicated genotypes (n=3 biologically independent experiments from 3 animals for each group; Data are mean ± SD; Tukey's pairwise comparison test; **P* < 0.05). **(d)** IHC staining for Mib1 (i; n=3 animals for each group; scale bar, 100 μm), the expression of *Ar* and *Esr2* **(e)** in MFs, and the mRNA expression of Notch target genes in MCs **(f)** (n=3 biologically independent experiments from 3 animals for each group; Data are mean ± SD; Two-sample *t*-test; **P* < 0.05).

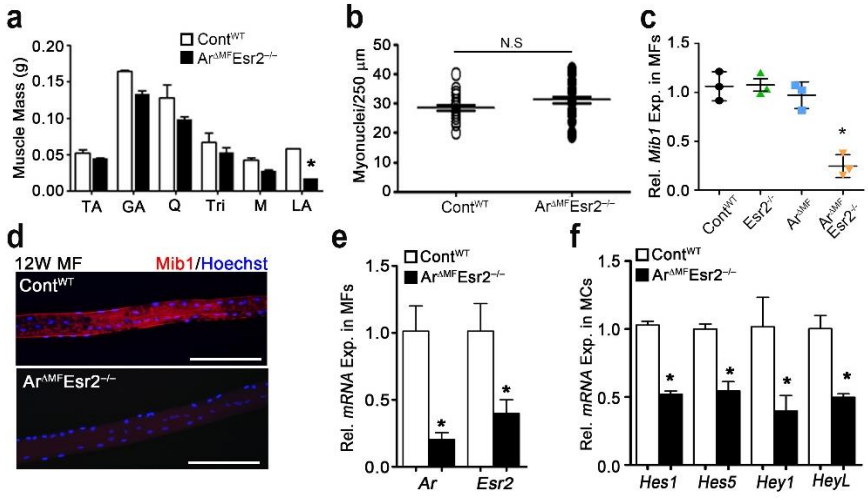
a
Cont^WT
Ar^ΔMFEsr2^−/−
Muscle Mass (g)
0.20
0.15
0.10
0.05
0.00
TA
GA
Q
Tri
M
LA
*
b
N.S
Myonuclei/250 μm
50
40
30
20
10
0
Cont^WT
Ar^ΔMFEsr2^−/−
c
Rel. Mib1 Exp. in MFs
1.5
1.0
0.5
0.0
*
Cont^WT
Esr2^−/−
Ar^ΔMF
Ar^ΔMF Esr2^−/−
d
12W MF
Mib1/Hoechst
Cont^WT
Ar^ΔMFEsr2^−/−
e
Cont^WT
Ar^ΔMFEsr2^−/−
Rel. mRNA Exp. in MFs
1.5
1.0
0.5
0.0
*
Ar
Esr2
f
Cont^WT
Ar^ΔMFEsr2^−/−
Rel. mRNA Exp. in MCs
1.5
1.0
0.5
0.0
*
Hes1
Hes5
Hey1
HeyL

Figure 29. Failure of *Mib1* induction by ablation of sex hormone receptors

(a,b) Serum testosterone (a) levels measured by ELISA and estradiol (b) levels measured by LC-MS/MS of 12-week-old $Cont^{WT}$, $Esr2^{-/-}$, $Ar^{\Delta MF}$ and $Ar^{\Delta MF}Esr2^{-/-}$ mice (n=3 biologically independent experiments from 3 animals for each group; Data are mean ± SD; Tukey's pairwise comparison test after ANOVA; $*P < 0.05$, N.S. not significant). **(c)** *Mib1* levels in MFs from 4-week-old TA muscles from indicated genotypes (n=3 biologically independent experiments from 200 myofibers for each group; Data are mean ± SD; Tukey's pairwise comparison test after ANOVA; N.S. not significant).

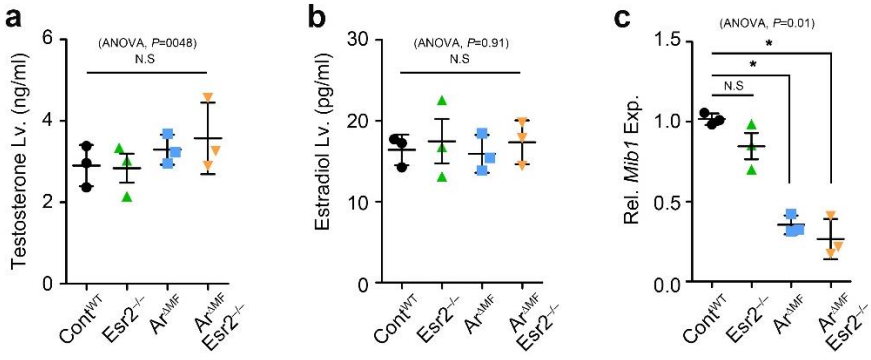
a
Testosterone Lv. (ng/ml)
(ANOVA, P=0048)
N.S
b
Estradiol Lv. (pg/ml)
(ANOVA, P=0.91)
N.S
c
Rel. Mib1 Exp.
(ANOVA, P=0.01)
N.S
*
*
Cont^WT
Esr2^-/-
Ar^ΔMF
Ar^ΔMF Esr2^-/-

Figure 30. Establishment of quiescent SCs via AR/ER induced *Mib1*-expressing MFs

(a) Representative IHC staining for Pax7 and Laminin in 8-week-old $Cont^{WT}$, $Esr2^{-/-}$, $Ar^{\Delta MF}$ and $Ar^{\Delta MF}Esr2^{-/-}$ TA muscles. Arrowheads indicate $Pax7^{+}$ cells. Controls are designated as the WT of comparing mutant mice (n=3 animals for each group; scale bar, 25 μm). **(b)** Quantification of Pax7 and Ki67 in TA muscles from the indicated genotypes and ages as in **a** (n=3 biologically independent experiments from 3 animals for each group; Data are mean ± SD; Tukey's pairwise comparison test; $*P < 0.05$; N.S. not significant). **(c)** Flow cytometric analysis of mononuclear cells from 8-week-old $Cont^{WT}$, $Esr2^{-/-}$, $Ar^{\Delta MF}$ and $Ar^{\Delta MF}Esr2^{-/-}$ hindlimb muscles. Controls are designated as the WT of comparing mutant mice (n=3 biologically independent experiments rom 3 animals for each group; Bootstrap *t*-test; $*P < 0.05$).

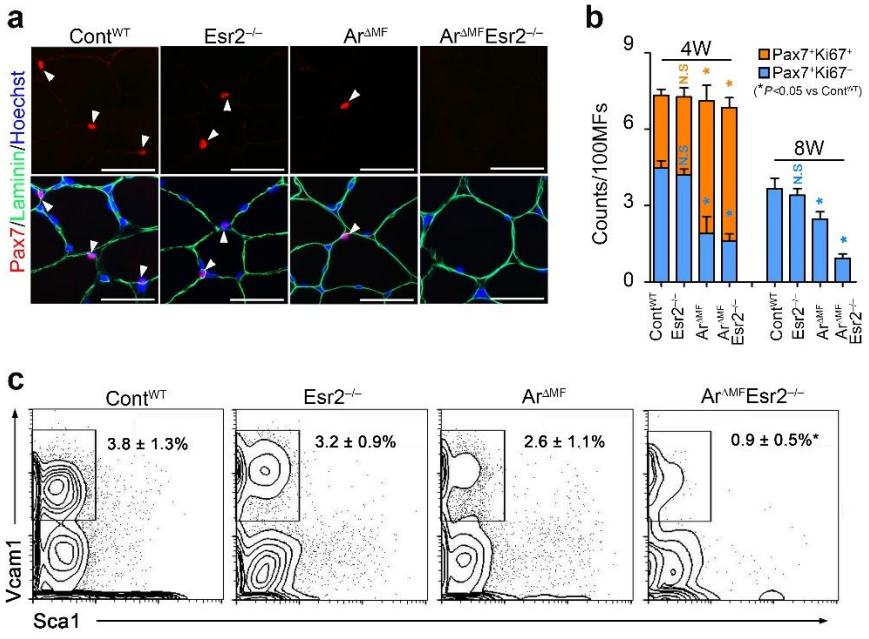
a
Cont^WT
Esr2^−/−
Ar^ΔMF
Ar^ΔMFEsr2^−/−
Pax7/Laminin/Hoechst
b
4W
8W
Pax7+Ki67+
Pax7+Ki67−
(*P<0.05 vs Cont^WT)
Counts/100MFs
N.S
c
3.8 ± 1.3%
3.2 ± 0.9%
2.6 ± 1.1%
0.9 ± 0.5%*
Vcam1
Sca1

Figure 31. Surgically and pharmacologically disturbed hypothalamic and gonadal axis impair the *Mib1* expression in MFs

(a) A schematic diagram for Nal-Lys gonadotropin releasing-hormone antagonist (Antide) injection or orchiectomy (Orx). **(b,c)** Serum testosterone levels measured by ELISA (b) and estradiol levels measured by LC-MS/MS (c) at indicated ages (n=3 biologically independent experiments from 3 animals for each group; Data are mean ± SD; Bootstrap *t*-test; $*P < 0.05$). **(d)** *Mib1* levels in MFs from Antide-treated or Orx mice pre-injected with Antide from 1-week-old or Orx at 2-week-old, respectively (n=3 biologically independent experiments from 3 animals for each group; Data are mean ± SD; Bootstrap *t*-test; $*P < 0.05$).

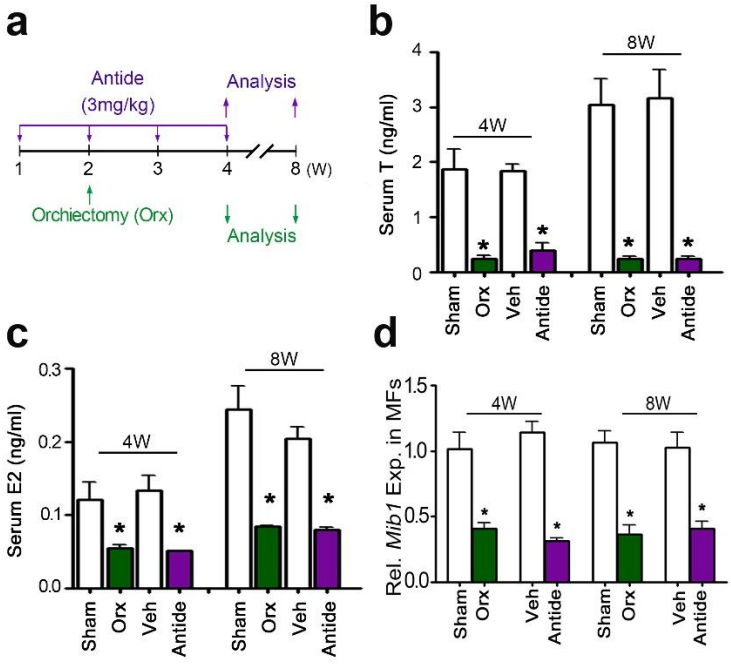
a
Antide
(3mg/kg)
Analysis
1
2
3
4
8 (W)
Orchiectomy (Orx)
Analysis
b
Serum T (ng/ml)
4W
8W
Sham
Orx
Veh
Antide
c
Serum E2 (ng/ml)
d
Rel. Mib1 Exp. in MFs

Figure 32. Establishment of adult SC populations by the hypothalamic-pituitary-gonadal axis

(a,b) IHC staining of Pax7 and Ki67 in TA muscles from 4-week-old Veh and Antide-treated mice (n=3 animals for each group; scale bar, 50 μm). **(c)**Quantification of Pax7 and Ki67 in TA muscles. (n=3 biologically independent experiments from 3 animals for each group; Data are mean ± SD; Bootstrap *t*-test; $*P < 0.05$).

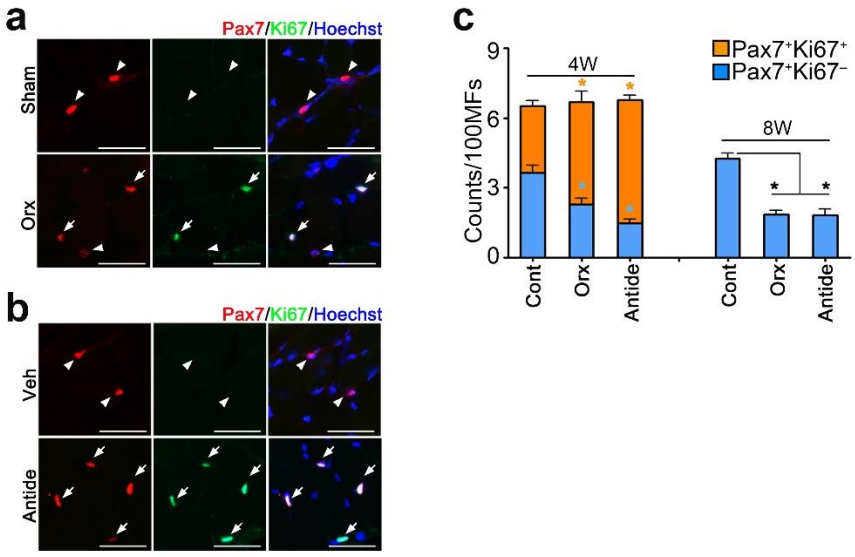
a
Pax7/Ki67/Hoechst
Sham
Orx
b
Pax7/Ki67/Hoechst
Veh
Antide
c
Pax7+Ki67+
Pax7+Ki67−
Counts/100MFs
9
6
3
0
4W
8W
Cont
Orx
Antide
Cont
Orx
Antide

Figure 33. Genetically disturbed models for hypothalamic and gonadal axis

(a-c) Gross morphology of seminal vesicles, testes and LA muscles (a; n=3 animals for each group; scale bar, 0.2 cm), muscle mass (b; n=3 animals for each group; Data are mean ± SD; Two-sample *t*-test; $*P < 0.05$) and myonuclei number of EDL muscles (c; n=3 biologically independent experiments from 3 animals for each group; Data are mean ± SD; Poisson's general linear model regression; N.S. not significant) in 8-week-old $Gnrh1^{+/+}$ and $Gnrh1^{hpg/hpg}$ mice. Muscle mass and myonuclei numbers were comparable in $Gnrh1^{+/+}$ and $Gnrh1^{hpg/hpg}$ mice.

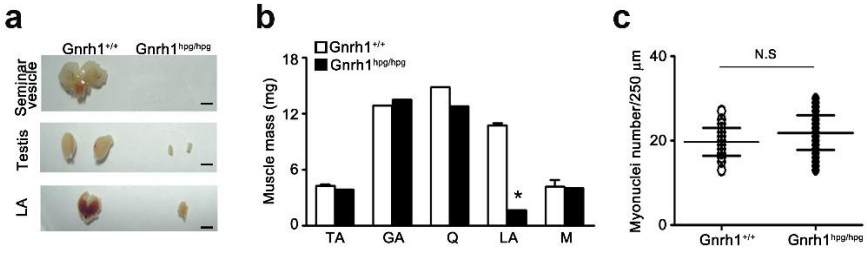
a
Gnrh1+/+
Gnrh1hpg/hpg
Seminal vesicle
Testis
LA
b
Gnrh1+/+
Gnrh1hpg/hpg
Muscle mass (mg)
18
12
6
0
TA
GA
Q
LA
M
*
c
N.S
Myonuclei number/250 μm
40
20
0
Gnrh1+/+
Gnrh1hpg/hpg

Figure 34. Defective Mib1 expression in MFs from hypogonadal mice by reduced production of sex hormones

(a,b) Serum testosterone levels measured by ELISA (a) and estradiol levels measured by LC-MS/MS (b) (n=3 biologically independent experiments; Data are mean ± SD; Bootstrap *t*-test; $*P < 0.05$). **(c)** Expression of *Mib1* in MFs from 8-week-old $Gnrh1^{+/+}$ and $Gnrh1^{hpg/hpg}$ mice (n=3 biologically independent experiments from 3 animals for each group; Data are mean ± SD; Bootstrap *t*-test; $*P < 0.05$).

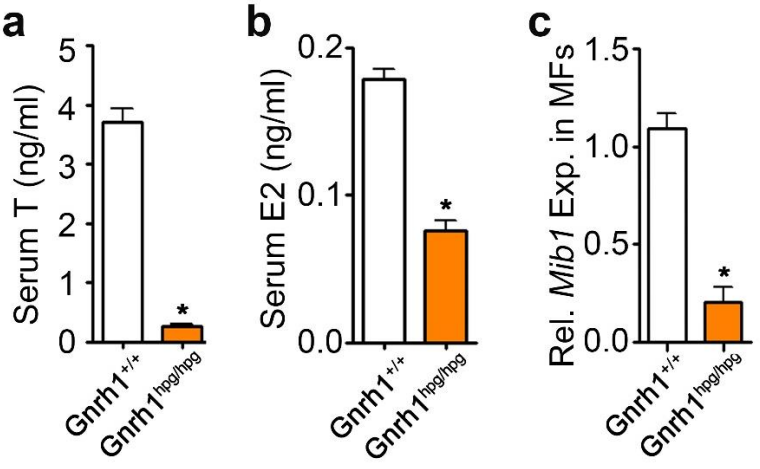
a
Serum T (ng/ml)
5
4
3
2
1
0
*
Gnrh1+/+
Gnrh1hpg/hpg
b
Serum E2 (ng/ml)
0.2
0.1
0.0
*
Gnrh1+/+
Gnrh1hpg/hpg
c
Rel. Mib1 Exp. in MFs
1.5
1.0
0.5
0.0
*
Gnrh1+/+
Gnrh1hpg/hpg

Figure 35. Establishment of adult SC populations by the hypothalamic-pituitary-gonadal axis

(a,b) The expression of *Ar* and *Esr2* in MFs (a) and Notch target genes in SCs (b) (n=3 biologically independent experiments from 3 animals for each group; Data are mean ± SD; Two-sample *t*-test; **P* < 0.05; ***P* < 0.01). **(c)** IHC staining (c) for Pax7 and Laminin in TA muscles. MFs, SCs, and TA muscles were isolated from 8-week-old $Gnrh1^{+/+}$ and $Gnrh1^{hpg/hpg}$ mice (n=3 animals for each group; scale bar, 50 μm). **(d)** Flow cytometric analysis of mononuclear cells from 8-week-old control (sum data of Sham, Veh, and $Gnrh1^{+/+}$), Orx, Antide-treated, and $Gnrh1^{hpg/hpg}$ hindlimb muscles (n=3 animals for each group; Data are mean ± SD; Bootstrap *t*-test; **P* < 0.05). **(e)** IHC staining of Pax7 in Vcam-1^{+}Sca-1^{-} cells sorted from mononuclear cells of $Gnrh1^{+/+}$ and $Gnrh1^{hpg/hpg}$ mice (n=3 animals for each group; scale bar, 50 μm).

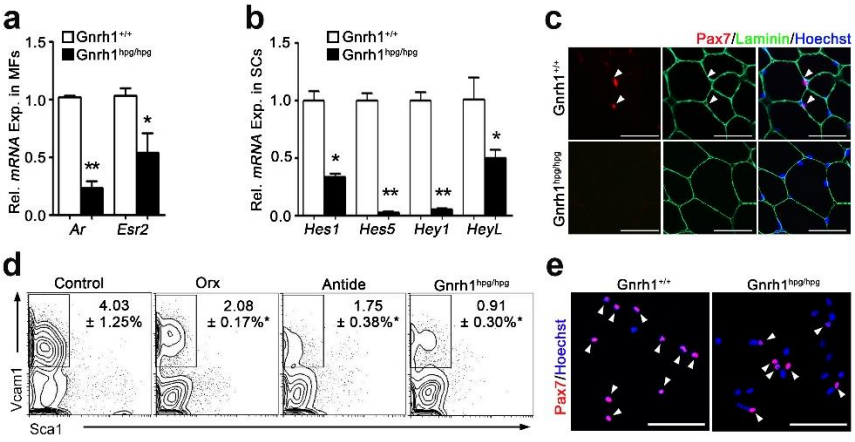
a
Gnrh1+/+
Gnrh1hpg/hpg
Rel. mRNA Exp. in MFs
1.5
1.0
0.5
0.0
**
*
Ar
Esr2
b
Gnrh1+/+
Gnrh1hpg/hpg
Rel. mRNA Exp. in SCs
1.5
1.0
0.5
0.0
*
**
**
*
Hes1
Hes5
Hey1
HeyL
c
Pax7/Laminin/Hoechst
Gnrh1+/+
Gnrh1hpg/hpg
d
Control
Orx
Antide
Gnrh1hpg/hpg
4.03
± 1.25%
2.08
± 0.17%*
1.75
± 0.38%*
0.91
± 0.30%*
Vcam1
Sca1
e
Gnrh1+/+
Gnrh1hpg/hpg
Pax7/Hoechst

Figure 36. Normal maintenance of QSC populations in short term inhibition of HPG axis

(a) A schematic diagram for Antide injection and Orx followed by $BaCl_2$-induced injury. (**b)** Gross morphology of *Levartor ani* (LA) muscles (n=5 animals for each group; scale bar, 0.5 cm). **(c)** Representative IHC staining for Pax7 and Laminin in uninjured mice. Arrowhead indicates $Pax7^+$ cells (n=5 animals for each group; scale bar, 50 μm). **(d)** Quantification of $Pax7^+$ cells in uninjured mice as in **c** (n=3 independent experiments from 5 animals for each group; Data are mean ± SD; One-Way ANOVA; N.S. not significant)

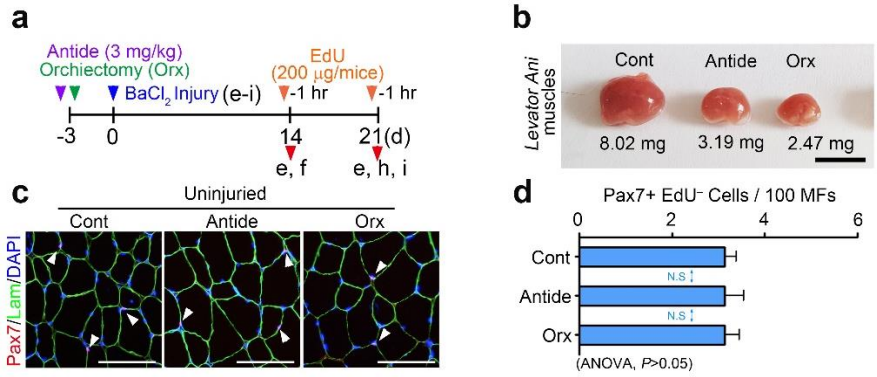
a
Antide (3 mg/kg)
Orchiectomy (Orx)
BaCl2 Injury (e-i)
EdU
(200 μg/mice)
-1 hr
-1 hr
-3
0
14
21(d)
e, f
e, h, i
b
Levator Ani muscles
Cont
Antide
Orx
8.02 mg
3.19 mg
2.47 mg
c
Uninjuried
Cont
Antide
Orx
Pax7/Lam/DAPI
d
Pax7+ EdU⁻ Cells / 100 MFs
0
2
4
6
Cont
Antide
Orx
N.S
N.S
(ANOVA, P>0.05)

Figure 37. Impaired re-establishment of SC populations in skeletal muscle regeneration

(a) Mean cross sectional area (CSA) of Laminin-stained TA muscles after 14 and 21 days of muscle injury. **(b)** Representative IHC staining for Pax7 and EdU of TA muscles after 14 days of muscle injury. Arrows and arrowheads indicate $Pax7^{+}EdU^{+}$ and $Pax7^{+}EdU^{-}$cells, respectively. **(c)** Quantification of $Pax7^{+}$ cells of TA muscles as in **b**. **(d)** Representative IHC staining for Pax7 and Laminin of TA muscles after 21 days of muscle injury. Arrowhead indicates $Pax7^{+}$ cells (n=5 animals for each group; scale bar, 25 μm). **(f)** Quantification of $Pax7^{+}EdU^{-}$ cells of TA muscles as in **d**. Arrows and arrowheads indicate $Pax7^{+}EdU^{+}$ and $Pax7^{+}EdU^{-}$cells, respectively (n=3 biologically independent experiments from 5 animals for each group; Data are mean ± SD; Kruskal-Wallis test; $*P < 0.05$, N.S. not significant).

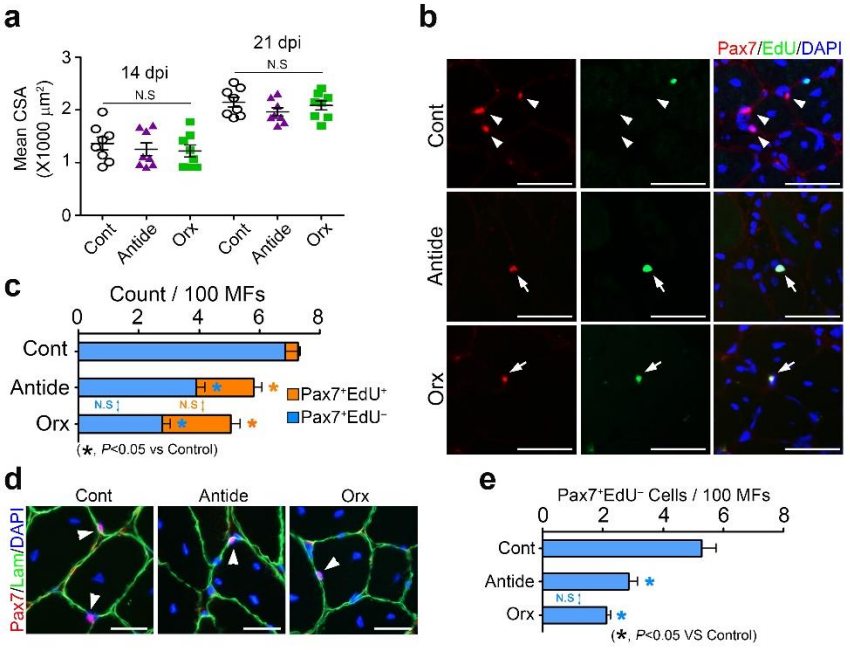
a
Mean CSA (X1000 μm²)
14 dpi
21 dpi
N.S
N.S
Cont
Antide
Orx
Cont
Antide
Orx
b
Pax7/EdU/DAPI
Cont
Antide
Orx
c
Count / 100 MFs
Cont
Antide
Orx
Pax7⁺EdU⁺
Pax7⁺EdU⁻
N.S
N.S
(*, P<0.05 vs Control)
d
Cont
Antide
Orx
Pax7/Lam/DAPI
e
Pax7⁺EdU⁻ Cells / 100 MFs
Cont
Antide
Orx
N.S
(*, P<0.05 VS Control)

Figure 38. Requirement of sex hormone in re-establishment of quiescent adult SC populations after muscle injury

(a) A schematic diagram for muscle regeneration of 12-week-old Orx mice implanted with DHT. **(b)** Gross morphology of LA muscles from control, Orx and Orx with DHT mice (n=5 animals for each group; scale bar, 0.5 cm). **(c)** Representative IHC staining for Pax7 and Laminin of TA muscles. Arrowhead indicates $Pax7^+$ cells (n=3 animals for each group; scale bar, 25 μm). **(d)** Quantification of $Pax7^+$ cells of TA muscles as in **c** (n=3 biologically independent experiments from 3 animals for each group; Data are mean ± SD; Bootstrap *t*-test, $*P < 0.05$). **(e)** Mean cross sectional area (CSA) of Laminin-stained TA muscles (n=3 biologically independent experiments from 5 animals for each group; Data are mean ± SD; one-way ANOVA; $*P < 0.05$).

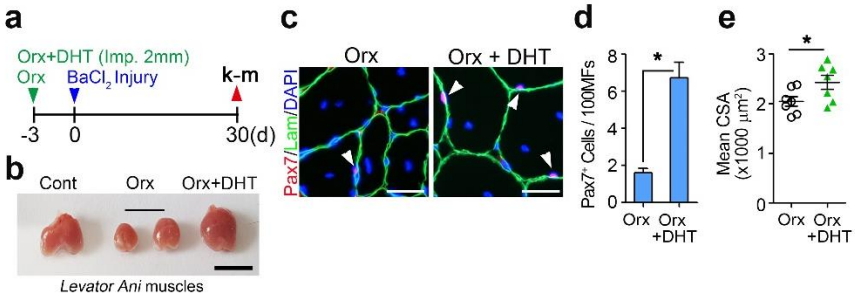
a
Orx+DHT (Imp. 2mm)
Orx
BaCl2 Injury
k-m
-3
0
30(d)
b
Cont
Orx
Orx+DHT
Levator Ani muscles
c
Orx
Orx + DHT
Pax7/Lam/DAPI
d
Pax7+ Cells / 100MFs
Orx
Orx +DHT
e
Mean CSA (x1000 μm2)
Orx
Orx +DHT

Figure 39. A proposed model

Active proliferation and differentiation of juvenile SCs contribute to myonuclear accretion in the pre-existing myofibers during the juvenile period. However, at puberty, the hypothalamic-pituitary-gonadal (HPG) axis is activated, leading to the secretion of gonadotropin-releasing hormone (Gnrh) from the hypothalamus, which subsequently increases the production of luteinizing hormone (LH) and follicle-stimulating hormone (FSH) in the pituitary gland. Consequently, LH and FSH promote the synthesis of estrogen and testosterone in the gonads. Notably, these increased levels of testosterone/DHT and E2 can independently induce Mib1 expression in MFs, allowing Mib1 to facilitate the ubiquitination and subsequent trans-endocytosis of the Notch ligands Delta1 and/or Jagged1 in MFs, which subsequently triggers Notch signaling in cycling SCs. Intriguingly, these converting SCs are withdrawn from the cell cycle and converted into adult quiescent SCs. Thereafter, the converting SCs preserve their stemness in order to comprise a reserve pool of adult stem cells. During regeneration, sex hormones may recover the Notch signaling for replenishment of quiescent satellite cell populations through the expression of Mib1 in regenerating MFs. In summary, hypothalamic-pituitary-gonadal-sex hormone-Mib1-Notch axis is an important regulator of establishment of quiescent adult SC pool at puberty and during muscle regeneration at adulthood.

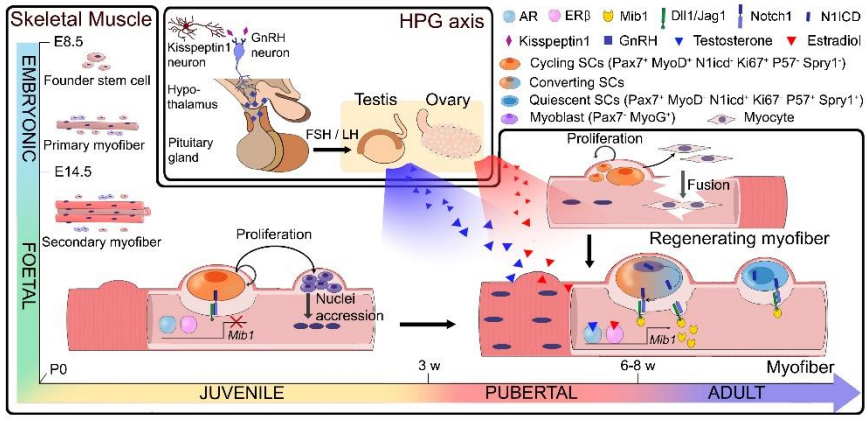
Skeletal Muscle
EMBRYONIC
FOETAL
E8.5
Founder stem cell
Primary myofiber
E14.5
Secondary myofiber
HPG axis
Kisspeptin1 neuron
GnRH neuron
Hypo-thalamus
Pituitary gland
FSH / LH
Testis
Ovary
AR
ERβ
Mib1
Dll1/Jag1
Notch1
N1ICD
Kisspeptin1
GnRH
Testosterone
Estradiol
Cycling SCs (Pax7+ MyoD+ N1icd- Ki67+ P57- Spry1+)
Converting SCs
Quiescent SCs (Pax7+ MyoD- N1icd- Ki67- P57+ Spry1+)
Myoblast (Pax7- MyoG+)
Myocyte
Proliferation
Nuclei accression
Mib1
Fusion
Regenerating myofiber
Myofiber
P0
3 w
6-8 w
JUVENILE
PUBERTAL
ADULT

V. DISCUSSION

Our results demonstrate the mechanism by which sex hormones establish the adult SC pool via regulation of Notch signaling at puberty. Both androgens and estrogens can independently induce Mib1 expression in MFs, and the Mib1-expressing MF niche is required for proliferating $Pax7^+$ juvenile SCs to exit the cell cycle and consequently establishes the quiescent $Pax7^+$ adult SC pool (Fig. 39). These sequential events reveal a mechanism that establishes the adult SC populations in skeletal muscles. Interestingly, the same mechanim is also applied to the replenishment of the SC pool after injury. Collectively, I conclude that the hypothalamic-pituitary-gonadal-sex hormone-Mib1-Notch axis is crucial for the establishment of quiescent SC pool not only at puberty, but also in regeneration upon injury at

adulthood. This mechanism secures some juvenile cycling SCs and activated SCs upon injury from myogenic differentiation flux and then establishes a reservoir pool of adult quiescent SCs that are required for the regeneration throughout life.

Males and females exhibit dimorphism of muscle mass and strength. However, they have equivalent ability to repair muscle damages albeit females have less number of adult SCs than males(Neal et al., 2012). In this study, I showed both sex hormones, T/DHT and E2, can independently and additively turn on Mib1 expression in muscle fibers (Fig. 24-26). Although T/DHT and E2 should function as major sex hormones in males and females, rescpetively(Ober et al., 2008), the net effect of circulating T and E2 would contribute to the induction of Mib1 in myofibers, suggesting how adult quiescent SC pools are established

in both sexes.

During postnatal growth, daughter cells of dividing SCs expressing Dll1 might send Notch signals to their sibling SCs, which leads to the retention of their proliferation and stemness(Conboy and Rando, 2002; Kuang et al., 2007). Otherwise, recent report suggests that forced expression of N1icd in fetal muscle progenitors causes them to exit the cell cycle(Mourikis et al., 2012a). Consistently, I observed that the overexpression of N1icd results in the conversion of cycling juvenile SCs into quiescent SCs (Fig. 12 and 13), whereas the deletion of Notch1 leads to impaired exit of the cell cycle in juvenile SCs (Fig. 9 and 10). In addition, specific disruption of Mib1 in myofibers failed to activate Notch1 signaling in juvenile SCs (Fig. 15-20), which impulse some proliferative SCs acquire the quiescence during puberty by receiving

Notch signals from their adjacent myofibers. At adulthood, the disruption of *RbpJ-κ* in quiescent SCs results in their terminal differentiation, suggesting that Notch signaling is active in quiescent SCs(Bjornson et al., 2012; Mourikis et al., 2012b). Our data, however, show that the adult quiescent SC populations can be maintained for a substantial period without sex hormones, suggesting a compensatory mechanism that retains Notch activity in adult SC, which makes adult SCs tolerate the circumstances of oscillating hormones in circadian/seasonal or estrous cyclic fluctuation(Lucas and Eleftheriou, 1980; Valdez et al., 2014; Zenclussen et al., 2014).

I showed in this study that sex hormones are essential for the re-establishment of quiescent SC populations in muscle regeneration at adulthood. In hormone rescue experiments (Fig. 38), I demonstrated

that DHT administration to Orx mice sufficiently and significantly restored the SC population after muscle regeneration (Fig. 8a-d). Consistent with our hormone replacement data, I speculate that the administration of additional E2 could repopulate the quiescent SCs as in hormone-reduced mice. This suggests the hypothalamic-pituitary-gonadal-sex hormone-Mib1-Notch axis as a promising therapeutic target for patients with hypogonadism or severe hormone deficiency caused by gonadectomy due to prostate cancer, genetic disorders, or age-associated diseases. Our findings demonstrate the potential therapeutic benefits of hormone treatment such as the restoration of quiescent SC pool and muscle homeostasis in repetitive activation and conversion of SCs throughout life. Consequently, this will shed a light on the understanding of muscle development, homeostasis, degeneration upon hormonal changes.

VI. REFERENCES

Al-Attar, L., Noel, K., Dutertre, M., Belville, C., Forest, M.G., Burgoyne, P.S., Josso, N., and Rey, R. (1997). Hormonal and cellular regulation of Sertoli cell anti-Mullerian hormone production in the postnatal mouse. J Clin Invest *100*, 1335-1343.

Bao, J., Ma, H.Y., Schuster, A., Lin, Y.M., and Yan, W. (2013). Incomplete cre-mediated excision leads to phenotypic differences between Stra8-iCre; Mov10l1(lox/lox) and Stra8-iCre; Mov10l1(lox/Delta) mice. Genesis *51*, 481-490.

Bentzinger, C.F., Wang, Y.X., and Rudnicki, M.A. (2012). Building muscle: molecular regulation of myogenesis. Cold Spring Harb Perspect Biol *4*.

Bhasin, S., Woodhouse, L., and Storer, T.W. (2003). Androgen effects on body composition. Growth Horm IGF Res *13 Suppl A*, S63-71.

Bjornson, C.R., Cheung, T.H., Liu, L., Tripathi, P.V., Steeper, K.M., and Rando, T.A. (2012). Notch signaling is necessary to maintain quiescence in adult muscle stem cells. Stem cells *30*, 232-242.

Bjornstrom, L., and Sjoberg, M. (2005). Mechanisms of estrogen receptor signaling: convergence of genomic and nongenomic actions on target genes. Mol Endocrinol *19*, 833-842.

Brack, A.S., Conboy, I.M., Conboy, M.J., Shen, J., and Rando, T.A. (2008). A temporal switch from notch to Wnt signaling in muscle stem cells is necessary for normal adult myogenesis. Cell stem cell *2*, 50-59.

Brohl, D., Vasyutina, E., Czajkowski, M.T., Griger, J., Rassek, C., Rahn, H.P., Purfurst, B., Wende, H., and Birchmeier, C. (2012). Colonization

of the satellite cell niche by skeletal muscle progenitor cells depends on Notch signals. Developmental cell *23*, 469-481.

Brown, D., Hikim, A.P., Kovacheva, E.L., and Sinha-Hikim, I. (2009). Mouse model of testosterone-induced muscle fiber hypertrophy: involvement of p38 mitogen-activated protein kinase-mediated Notch signaling. The Journal of endocrinology *201*, 129-139.

Bruning, J.C., Michael, M.D., Winnay, J.N., Hayashi, T., Horsch, D., Accili, D., Goodyear, L.J., and Kahn, C.R. (1998). A muscle-specific insulin receptor knockout exhibits features of the metabolic syndrome of NIDDM without altering glucose tolerance. Mol Cell *2*, 559-569.

Camarda, G., Siepi, F., Pajalunga, D., Bernardini, C., Rossi, R., Montecucco, A., Meccia, E., and Crescenzi, M. (2004). A pRb-independent mechanism preserves the postmitotic state in terminally differentiated skeletal muscle cells. The Journal of cell biology *167*, 417-423.

Carson, J.A., Lee, W.J., McClung, J., and Hand, G.A. (2002). Steroid receptor concentration in aged rat hindlimb muscle: effect of anabolic steroid administration. J Appl Physiol *93*, 242-250.

Cattanach, B.M., Iddon, C.A., Charlton, H.M., Chiappa, S.A., and Fink, G. (1977). Gonadotrophin-releasing hormone deficiency in a mutant mouse with hypogonadism. Nature *269*, 338-340.

Chakkalakal, J.V., Jones, K.M., Basson, M.A., and Brack, A.S. (2012). The aged niche disrupts muscle stem cell quiescence. Nature *490*, 355-360.

Chambon, C., Duteil, D., Vignaud, A., Ferry, A., Messaddeq, N., Malivindi, R., Kato, S., Chambon, P., and Metzger, D. (2010). Myocytic androgen receptor controls the strength but not the mass of limb muscles. Proceedings of the National Academy of Sciences of the

United States of America *107*, 14327-14332.
Conboy, I.M., and Rando, T.A. (2002). The regulation of Notch signaling controls satellite cell activation and cell fate determination in postnatal myogenesis. Dev Cell *3*, 397-409.
Davis, T.A., and Fiorotto, M.L. (2009). Regulation of muscle growth in neonates. Curr Opin Clin Nutr Metab Care *12*, 78-85.
Doumit, M.E., Cook, D.R., and Merkel, R.A. (1996). Testosterone up-regulates androgen receptors and decreases differentiation of porcine myogenic satellite cells in vitro. Endocrinology *137*, 1385-1394.
Dupont, S., Krust, A., Gansmuller, A., Dierich, A., Chambon, P., and Mark, M. (2000). Effect of single and compound knockouts of estrogen receptors alpha (ERalpha) and beta (ERbeta) on mouse reproductive phenotypes. Development *127*, 4277-4291.
Ebling, F.J. (2005). The neuroendocrine timing of puberty. Reproduction *129*, 675-683.
Edelstein, M.C., Gordon, K., Williams, R.F., Danforth, D.R., and Hodgen, G.D. (1990). Single dose long-term suppression of testosterone secretion by a gonadotropin-releasing hormone antagonist (Antide) in male monkeys. Contraception *42*, 209-214.
Fre, S., Huyghe, M., Mourikis, P., Robine, S., Louvard, D., and Artavanis-Tsakonas, S. (2005). Notch signals control the fate of immature progenitor cells in the intestine. Nature *435*, 964-968.
Fukada, S., Uezumi, A., Ikemoto, M., Masuda, S., Segawa, M., Tanimura, N., Yamamoto, H., Miyagoe-Suzuki, Y., and Takeda, S. (2007). Molecular signature of quiescent satellite cells in adult skeletal muscle. Stem cells *25*, 2448-2459.
Gibson, M.C., and Schultz, E. (1983). Age-related differences in absolute numbers of skeletal muscle satellite cells. Muscle Nerve *6*,

574-580.

Gunther, S., Kim, J., Kostin, S., Lepper, C., Fan, C.M., and Braun, T. (2013). Myf5-Positive Satellite Cells Contribute to Pax7-Dependent Long-Term Maintenance of Adult Muscle Stem Cells. Cell Stem Cell.

Jeong, H.W., Jeon, U.S., Koo, B.K., Kim, W.Y., Im, S.K., Shin, J., Cho, Y., Kim, J., and Kong, Y.Y. (2009). Inactivation of Notch signaling in the renal collecting duct causes nephrogenic diabetes insipidus in mice. J Clin Invest *119*, 3290-3300.

Jeong, H.W., Kim, J.H., Kim, J.Y., Ha, S.J., and Kong, Y.Y. (2012). Mind Bomb-1 in Dendritic Cells Is Specifically Required for Notch-mediated T Helper Type 2 Differentiation. PLoS One *7*, e36359.

Kadi, F., Bonnerud, P., Eriksson, A., and Thornell, L.E. (2000). The expression of androgen receptors in human neck and limb muscles: effects of training and self-administration of androgenic-anabolic steroids. Histochem Cell Biol *113*, 25-29.

Kalbe, C., Mau, M., Wollenhaupt, K., and Rehfeldt, C. (2007). Evidence for estrogen receptor alpha and beta expression in skeletal muscle of pigs. Histochemistry and cell biology *127*, 95-107.

Kim, Y.W., Koo, B.K., Jeong, H.W., Yoon, M.J., Song, R., Shin, J., Jeong, D.C., Kim, S.H., and Kong, Y.Y. (2008). Defective Notch activation in microenvironment leads to myeloproliferative disease. Blood *112*, 4628-4638.

Koo, B.K., Lim, H.S., Song, R., Yoon, M.J., Yoon, K.J., Moon, J.S., Kim, Y.W., Kwon, M.C., Yoo, K.W., Kong, M.P.*, et al.* (2005). Mind bomb 1 is essential for generating functional Notch ligands to activate Notch. Development *132*, 3459-3470.

Koo, B.K., Yoon, M.J., Yoon, K.J., Im, S.K., Kim, Y.Y., Kim, C.H., Suh, P.G., Jan, Y.N., and Kong, Y.Y. (2007). An obligatory role of mind bomb-

1 in notch signaling of mammalian development. PLoS One *2*, e1221.
Kopan, R., and Ilagan, M.X. (2009). The canonical Notch signaling pathway: unfolding the activation mechanism. Cell *137*, 216-233.
Kuang, S., Kuroda, K., Le Grand, F., and Rudnicki, M.A. (2007). Asymmetric self-renewal and commitment of satellite stem cells in muscle. Cell *129*, 999-1010.
Lepper, C., and Fan, C.M. (2010). Inducible lineage tracing of Pax7-descendant cells reveals embryonic origin of adult satellite cells. Genesis *48*, 424-436.
Lepper, C., Partridge, T.A., and Fan, C.M. (2011). An absolute requirement for Pax7-positive satellite cells in acute injury-induced skeletal muscle regeneration. Development *138*, 3639-3646.
Liu, L., Cheung, T.H., Charville, G.W., Hurgo, B.M., Leavitt, T., Shih, J., Brunet, A., and Rando, T.A. (2013). Chromatin modifications as determinants of muscle stem cell quiescence and chronological aging. Cell reports *4*, 189-204.
Liu, L., Cheung, T.H., Charville, G.W., and Rando, T.A. (2015). Isolation of skeletal muscle stem cells by fluorescence-activated cell sorting. Nature protocols *10*, 1612-1624.
Lucas, L.A., and Eleftheriou, B.E. (1980). Circadian variation in concentrations of testosterone in the plasma of male mice: a difference between BALB/cBy and C57BL/6By inbred strains. The Journal of endocrinology *87*, 37-46.
Maatta, J.A., Buki, K.G., Ivaska, K.K., Nieminen-Pihala, V., Elo, T.D., Kahkonen, T., Poutanen, M., Harkonen, P., and Vaananen, K. (2013). Inactivation of the androgen receptor in bone-forming cells leads to trabecular bone loss in adult female mice. Bonekey Rep *2*, 440.
MacLean, H.E., and Handelsman, D.J. (2009). Unraveling androgen

action in muscle: genetic tools probing cellular mechanisms. Endocrinology *150*, 3437-3439.

Marino, M., Galluzzo, P., and Ascenzi, P. (2006). Estrogen signaling multiple pathways to impact gene transcription. Curr Genomics *7*, 497-508.

Moon, J.Y., Kim, K.J., Moon, M.H., Chung, B.C., and Choi, M.H. (2011). A novel GC-MS method in urinary estrogen analysis from postmenopausal women with osteoporosis. Journal of lipid research *52*, 1595-1603.

Mourikis, P., Gopalakrishnan, S., Sambasivan, R., and Tajbakhsh, S. (2012a). Cell-autonomous Notch activity maintains the temporal specification potential of skeletal muscle stem cells. Development *139*, 4536-4548.

Mourikis, P., Sambasivan, R., Castel, D., Rocheteau, P., Bizzarro, V., and Tajbakhsh, S. (2012b). A critical requirement for notch signaling in maintenance of the quiescent skeletal muscle stem cell state. Stem cells *30*, 243-252.

Murtaugh, L.C., Stanger, B.Z., Kwan, K.M., and Melton, D.A. (2003). Notch signaling controls multiple steps of pancreatic differentiation. Proceedings of the National Academy of Sciences of the United States of America *100*, 14920-14925.

Neal, A., Boldrin, L., and Morgan, J.E. (2012). The satellite cell in male and female, developing and adult mouse muscle: distinct stem cells for growth and regeneration. PloS one *7*, e37950.

Ober, C., Loisel, D.A., and Gilad, Y. (2008). Sex-specific genetic architecture of human disease. Nature reviews Genetics *9*, 911-922.

Ohkawa, Y., Mallappa, C., Vallaster, C.S., and Imbalzano, A.N. (2012). Isolation of nuclei from skeletal muscle satellite cells and myofibers for

use in chromatin immunoprecipitation assays. Methods in molecular biology *798*, 517-530.

Parker, M.H., Seale, P., and Rudnicki, M.A. (2003). Looking back to the embryo: defining transcriptional networks in adult myogenesis. Nat Rev Genet *4*, 497-507.

Pellettieri, J., and Sanchez Alvarado, A. (2007). Cell turnover and adult tissue homeostasis: from humans to planarians. Annu Rev Genet *41*, 83-105.

Pinter O., B.Z., Csaba Z. & Gerendai I. (2007). Differences in the onset of puberty in selected inbred mouse strains. Endocr Abstr *14*, 617.

Rios, A.C., Serralbo, O., Salgado, D., and Marcelle, C. (2011). Neural crest regulates myogenesis through the transient activation of NOTCH. Nature *473*, 532-535.

Roubinian, J.R., Talal, N., Greenspan, J.S., Goodman, J.R., and Siiteri, P.K. (1978). Effect of castration and sex hormone treatment on survival, anti-nucleic acid antibodies, and glomerulonephritis in NZB/NZW F1 mice. The Journal of experimental medicine *147*, 1568-1583.

Safranski, T.J., Lamberson, W.R., and Keisler, D.H. (1993). Correlations among three measures of puberty in mice and relationships with estradiol concentration and ovulation. Biology of reproduction *48*, 669-673.

Sambasivan, R., and Tajbakhsh, S. (2007). Skeletal muscle stem cell birth and properties. Semin Cell Dev Biol *18*, 870-882.

Sambasivan, R., Yao, R., Kissenpfennig, A., Van Wittenberghe, L., Paldi, A., Gayraud-Morel, B., Guenou, H., Malissen, B., Tajbakhsh, S., and Galy, A. (2011). Pax7-expressing satellite cells are indispensable for adult skeletal muscle regeneration. Development *138*, 3647-3656.

Schmalbruch, H., and Lewis, D.M. (2000). Dynamics of nuclei of muscle

fibers and connective tissue cells in normal and denervated rat muscles. Muscle Nerve *23*, 617-626.

Schultz, E. (1996). Satellite cell proliferative compartments in growing skeletal muscles. Dev Biol *175*, 84-94.

Schuster-Gossler, K., Cordes, R., and Gossler, A. (2007). Premature myogenic differentiation and depletion of progenitor cells cause severe muscle hypotrophy in Delta1 mutants. Proceedings of the National Academy of Sciences of the United States of America *104*, 537-542.

Shea, K.L., Xiang, W., LaPorta, V.S., Licht, J.D., Keller, C., Basson, M.A., and Brack, A.S. (2010). Sprouty1 regulates reversible quiescence of a self-renewing adult muscle stem cell pool during regeneration. Cell stem cell *6*, 117-129.

Shiina, H., Matsumoto, T., Sato, T., Igarashi, K., Miyamoto, J., Takemasa, S., Sakari, M., Takada, I., Nakamura, T., Metzger, D.*, et al.* (2006). Premature ovarian failure in androgen receptor-deficient mice. Proceedings of the National Academy of Sciences of the United States of America *103*, 224-229.

Sinha-Hikim, I., Taylor, W.E., Gonzalez-Cadavid, N.F., Zheng, W., and Bhasin, S. (2004). Androgen receptor in human skeletal muscle and cultured muscle satellite cells: up-regulation by androgen treatment. J Clin Endocrinol Metab *89*, 5245-5255.

Song, R., Kim, Y.W., Koo, B.K., Jeong, H.W., Yoon, M.J., Yoon, K.J., Jun, D.J., Im, S.K., Shin, J., Kong, M.P.*, et al.* (2008). Mind bomb 1 in the lymphopoietic niches is essential for T and marginal zone B cell development. J Exp Med *205*, 2525-2536.

Song, R., Koo, B.K., Yoon, K.J., Yoon, M.J., Yoo, K.W., Kim, H.T., Oh, H.J., Kim, Y.Y., Han, J.K., Kim, C.H.*, et al.* (2006). Neuralized-2 regulates a Notch ligand in cooperation with Mind bomb-1. J Biol Chem

281, 36391-36400.

Sun, J., Huang, Y.R., Harrington, W.R., Sheng, S., Katzenellenbogen, J.A., and Katzenellenbogen, B.S. (2002). Antagonists selective for estrogen receptor alpha. Endocrinology *143*, 941-947.

Tajbakhsh, S. (2009). Skeletal muscle stem cells in developmental versus regenerative myogenesis. J Intern Med *266*, 372-389.

Tajbakhsh, S., Rocancourt, D., Cossu, G., and Buckingham, M. (1997). Redefining the genetic hierarchies controlling skeletal myogenesis: Pax-3 and Myf-5 act upstream of MyoD. Cell *89*, 127-138.

Valdez, D.J., Vera Cortez, M., Della Costa, N.S., Leche, A., Hansen, C., Navarro, J.L., and Martella, M.B. (2014). Seasonal changes in plasma levels of sex hormones in the greater Rhea (Rhea americana), a South American Ratite with a complex mating system. PloS one *9*, e97334.

Van Uytfanghe, K., Stockl, D., Kaufman, J.M., Fiers, T., Ross, H.A., De Leenheer, A.P., and Thienpont, L.M. (2004). Evaluation of a candidate reference measurement procedure for serum free testosterone based on ultrafiltration and isotope dilution-gas chromatography-mass spectrometry. Clinical chemistry *50*, 2101-2110.

Vasyutina, E., Lenhard, D.C., Wende, H., Erdmann, B., Epstein, J.A., and Birchmeier, C. (2007). RBP-J (Rbpsuh) is essential to maintain muscle progenitor cells and to generate satellite cells. Proc Natl Acad Sci U S A *104*, 4443-4448.

Velders, M., Schleipen, B., Fritzemeier, K.H., Zierau, O., and Diel, P. (2012). Selective estrogen receptor-beta activation stimulates skeletal muscle growth and regeneration. FASEB journal : official publication of the Federation of American Societies for Experimental Biology *26*, 1909-1920.

Weinmaster, G., and Fischer, J.A. (2011). Notch ligand ubiquitylation:

what is it good for? Dev Cell *21*, 134-144.

Weiser, M.J., Wu, T.J., and Handa, R.J. (2009). Estrogen receptor-beta agonist diarylpropionitrile: biological activities of R- and S-enantiomers on behavior and hormonal response to stress. Endocrinology *150*, 1817-1825.

White, R.B., Bierinx, A.S., Gnocchi, V.F., and Zammit, P.S. (2010). Dynamics of muscle fibre growth during postnatal mouse development. BMC developmental biology *10*, 21.

Wierman, M.E. (2007). Sex steroid effects at target tissues: mechanisms of action. Adv Physiol Educ *31*, 26-33.

Wiik, A., Ekman, M., Johansson, O., Jansson, E., and Esbjornsson, M. (2009). Expression of both oestrogen receptor alpha and beta in human skeletal muscle tissue. Histochemistry and cell biology *131*, 181-189.

Xu, X., Keefer, L.K., Ziegler, R.G., and Veenstra, T.D. (2007). A liquid chromatography-mass spectrometry method for the quantitative analysis of urinary endogenous estrogen metabolites. Nature protocols *2*, 1350-1355.

Yang, X., Klein, R., Tian, X., Cheng, H.T., Kopan, R., and Shen, J. (2004). Notch activation induces apoptosis in neural progenitor cells through a p53-dependent pathway. Developmental biology *269*, 81-94.

Yoo, Y.E., and Ko, C.P. (2012). Dihydrotestosterone ameliorates degeneration in muscle, axons and motoneurons and improves motor function in amyotrophic lateral sclerosis model mice. PloS one *7*, e37258.

Yoon, K.J., Koo, B.K., Im, S.K., Jeong, H.W., Ghim, J., Kwon, M.C., Moon, J.S., Miyata, T., and Kong, Y.Y. (2008a). Mind bomb 1-expressing intermediate progenitors generate notch signaling to maintain radial glial cells. Neuron *58*, 519-531.

Yoon, M.J., Koo, B.K., Song, R., Jeong, H.W., Shin, J., Kim, Y.W., Kong, Y.Y., and Suh, P.G. (2008b). Mind bomb-1 is essential for intraembryonic hematopoiesis in the aortic endothelium and the subaortic patches. Mol Cell Biol *28*, 4794-4804.

Zenclussen, M.L., Casalis, P.A., Jensen, F., Woidacki, K., and Zenclussen, A.C. (2014). Hormonal Fluctuations during the Estrous Cycle Modulate Heme Oxygenase-1 Expression in the Uterus. Frontiers in endocrinology *5*, 32.

VII. 국문 초록

근육은 우리 몸을 구성하는 가장 큰 장기로써, 일생 동안 끊임 없이 파괴와 재생을 반복한다. 위성 세포로도 잘 알려진 성체 근육 줄기세포는 뚜렷한 골격근의 재형성 및 재생 능력에 관여함으로써, 근육의 항상성 유지에 있어서 중요한 역할을 한다. 이러한 위성세포는 배아기 중배엽의 체절에서부터 기원하는 다분화능 줄기/기원 세포로부터 유래됨에도 불구하고, 휴지기 성체 근육줄기세포의 형성에 관련된 기작은 알려져 있지 않다.

나는 이번 연구에서 성호르몬이 근육 섬유 내부에서 Notch 신호 관련 E3 접합체인 Mib1의 발현을 사춘기 시기에서부터 유도함으로써 활성화된 유아기 근육 줄기세포를 성숙한 성체 줄기세포로 유지한다는 사실을 밝혔다. 특히 Mib1 결핍 근섬유는 유아기 활성 근육 줄기세포로 Notch 신호를 전달하지 못하고,

결과적으로 근육 줄기세포를 휴지기로 유도하지 못하게 된다. Notch 결핍 활성 줄기세포는 분화 단계로 들어서게 되고 결국 성체 근육 줄기세포의 형성이 불가능하게 된다. 우리의 발견은 시상하부-뇌하수체-생식선 축이 근육 섬유 내부의 Mib1의 발현을 유도한다는 것을 확인한 것이다. 이러한 시상하부-뇌하수체-생식선 축은 근육 재생 이후에 근육 줄기세포의 재형성에도 관여함을 규명하였다. 결과적으로 성호르몬은 사춘기시기의 활성 줄기세포를 성체 줄기세포로 유도하여 근육 섬유 위에서 휴지기로 유지 하며, 같은 분자적 기작을 통하여 근육 손상 이후 활성화된 줄기세포의 항상성을 조절한다는 결론을 얻을 수 있었다.

Key word: Adult muscle stem cells (Satellite cells), Myofibers, Sex hormones, Puberty, Notch signaling pathway, Mind-Bomb1 (Mib1)

Student Number: 2009-2292